Applied Energy 392 (2025) 125937

Contents lists available at ScienceDirect

Applied Energy

journal homepage: www.elsevier.com/locate/apenergy

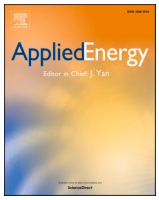

A multi-scenario distributionally robust model for resilience-oriented offshore wind farms and transmission network integrated planning considering typhoon disasters☆

Yang Yuan [a], Heng Zhang [a,*], Shenxi Zhang [a], Haozhong Cheng [a], Fangping Chen [b], Zheng Wang [c], Xiaohu Zhang [c]

[a] Key Laboratory of Control of Power Transmission and Conversion, Ministry of Education (Shanghai Jiao Tong University), Shanghai 200240, China
[b] Wukong Lab, IKINGTEC CO., Ltd, Beijing 100871, China
[c] East China Power Grid Company, Shanghai 200002, China

HIGHLIGHTS

- The multi-scenario distributionally robust uncertainty sets for wind farm outputs and grid faults.
- An offshore wind farms and transmission network integrated planning model considering normal and typhoon scenarios.
- A differential hardening model and its integration with the planning model.

ARTICLE INFO

Keywords:
Distributionally robust
Offshore wind farm
Planning
Resilience
Typhoon
Transmission network

ABSTRACT

Existing resilience-oriented offshore wind farms and transmission network integrated planning (ROWF&TNIP) models lack detailed characterization of the uncertainties associated with wind power and grid faults during typhoon disasters, and tend to be relatively conservative in enhancing resilience. To address these limitations, this paper proposes a multi-scenario distributionally robust model for ROWF&TNIP considering typhoon disasters. This model accounts for multiple uncertainties in wind power and grid faults under both normal operation scenario (NOS) and typhoon disaster scenario (TDS), and enhances resilience in a less conservative manner. Firstly, the multi-scenario distributionally robust uncertainty sets for offshore wind farms (OWF) output and grid fault are established: a conditional value-at-risk (CVaR) based multi-scenario budget uncertainty set to capture the uncertainties of wind turbine outputs and turbine failures under NOS and TDS, and a 1-norm grid fault uncertainty set to represent the uncertain probability distribution of four types of fault: high-probability faults, high-loss faults, cascading faults under TDS and fault-free state under NOS. Subsequently, a multi-scenario distributionally robust ROWF&TNIP model is formulated, utilizing the worst-case expected load-shedding cost under TDS as resilience index, the planning and expected generation cost under TDS and NOS as economic index. This model coordinates resilience and economic efficiency under the most adverse realization of uncertain OWF outputs and grid faults. To further mitigate the conservatism of the ROWF&TNIP model, short-term source-grid-load measures, including preventive unit commitment, differential load-shedding and an innovative differential hardening model, are integrated to the planning model. A column and constraint generation (C&CG) based decomposition algorithm is developed to solve the model. In case study section, a series of comparative and sensitivity analyses are conducted on the IEEE-30 bus system and a Chinese 81-bus system to demonstrate the effectiveness of the proposed model and reveal how key parameters of the model influence the resilience and economy of the planning results.

☆ This work was sponsored by National Natural Science Foundation of China (No. U23B6006, 52307120).

* Corresponding author at: Key Laboratory of Control of Power Transmission and Conversion, Ministry of Education, Electrical Engineering Department, Shanghai Jiao Tong University, Shanghai, China.
E-mail address: zhangheng_sjtu@sjtu.edu.cn (H. Zhang).

https://doi.org/10.1016/j.apenergy.2025.125937
Received 10 September 2024; Received in revised form 15 March 2025; Accepted 11 April 2025
Available online 2 May 2025

1. Introduction

Traditioanlly, offshore wind farms and transmission network integrated planning (OWF&TNIP) mainly focus on the economy and reliability of planning schemes. However, in recent years, the frequent occurrence of high-impact, low-probability (HILP) extreme events such as typhoons, earthquakes, and floods has posed significant challenges to power system planning and operation and drawn researchers' attention to the resilience of power system [1]. The difference between reliability and resilience lies in that the former focuses on the system's ability to provide stable power supply under long-term, normal operating conditions, while the latter emphasizes the system's ability to prevent, resist, absorb, and recover from short-term, HILP extreme events [2]. OWF&TNIP with resilience enhancement as the goal is referred to as ROWF&TNIP. Different types of disasters have distinct disaster-inducing mechanisms and impacts on power system. For ROWF&TNIP considering typhoon disasters, two issues are particularly noteworthy. Firstly, in comparison to NOS, the randomness, intermittency, and volatility of.

wind power intensify in TDS, accompanied by an evident increase in the probability and uncertainty of grid failures. Consequently, a pivotal challenge in ROWF&TNIP lies in how to effectively model the uncertainties associated with wind power and grid failures in TDS. Secondly, OWF&TNIP represents a long-term measure that requires significant investment [3]. In contrast, typhoon disasters are short-term events. Hence, a crucial issue in ROWF&TNIP is how to coordinate planning measures with various short-term resilience enhancement strategies, such as transmission line hardening, while simultaneously balancing economic objectives in NOS, to prevent overly conservative planning scheme and excessive investment. In the following sections, we present an overview of the current research status, research gaps, and our contributions pertaining to these issues.

1.1. Uncertainty model for wind farm output and grid fault under typhoon overview

Existing wind farm output uncertainty models can be classified into two categories: the multi-scenario or stochastic optimization-based models, which utilize historical data to construct typical scenarios of wind farm output [4]; and the robust or distributionally robust optimization-based models, which construct various uncertainty sets for wind farm output [5–8]. [5,6] are robust optimization-based, both employing the budget uncertainty set to captures the uncertain fluctuation range of wind farm output. The difference between [5,6] is that [6] establishes both day-ahead and intra-day budget uncertainty sets for wind farm output, whereas [5] only creates a single budget uncertainty set [7,8] are distributionally robust optimization-based, both employing distance-based ambiguity sets to characterize probability distribution uncertainty. The difference between [7,8] lies in that [7] utilizes ϕ-divergence-based ambiguity set to depict the uncertain probability distribution of wind farm maintenance demand, whereas [8] applies Wasserstein distance-based ambiguity set to model the uncertain probability distribution of typhoon parameters and the corresponding wind farm output. Robust or distributionally robust uncertainty sets do not rely on large amount of historical data or precise probabilistic models, and they can facilitate the identification of extreme scenarios for further optimization. These advantages are particularly suited to resilience-oriented optimization considering extreme events like typhoon disasters. However, it is inappropriate to simply applying the uncertainty models in [5–8] to ROWF&TNIP considering typhoon disasters. On one hand, [5–8] neglect the risk of wind turbine failures which may significantly increase during typhoon. Although there are models regarding the risk of turbine failures during typhoon, for example, [9] examines the influence of wind velocity on the turbine failure rate, these models are deterministic, ignoring the uncertain turbine failures during typhoon. On the other, [5–8] focus on short-term operation optimization problems, so that they can ignore the differences in wind farm output uncertainty between normal and typhoon scenarios. However, for long-term ROWF&TNIP problems, this issue should not be ignored.

For grid fault model, characterizing component failure rate and possible fault scenarios under typhoon disasters are two primary considerations. On one hand, researchers have developed detailed deterministic data/model-driven component failure rate models. [10] merely focuses on the fragility curve of the overhead lines, while [11] accounts for the influence of cascading faults on line failure rate. [12] leverage data mining to predict component failure rate under extreme weather. However, [10–12] assume that the component failure rate can be accurately calculated based on significant historical data or theoretical assumption, which may not be feasible for HILP events like typhoon disasters which are highly uncertain and lacks of historical data. The state-of-art research [13] utilizes distributionally robust method to model the failure rate uncertainty of single component, but the uncertain probability of combined failures involving multiple components has not been addressed. On the other hand, in terms of fault scenario models, existing works are either scenario-based, relying on various representative fault scenario generation methods, such as Markov process [14], complex network theory [15], Monte Carlo simulation [16], or robust optimization-based, identifying the worst-case fault scenarios within a typhoon-related contingency set [17,18]. Specially, the robust optimization-based models are widely used in resilience-oriented planning to search the high-loss faults in HILP event. However, these approaches often center on one type of fault scenarios such as severe faults or cascading faults, overlooking the diverse types of fault scenarios and the uncertain possibility of these fault scenarios under TDS. In summary, there is a need for further research on modeling the uncertainties in both component failure rate and fault scenarios during typhoon disasters.

1.2. Planning model integrated with other resilience enhancement measures overview

To reduce the conservatism of planning schemes and avoid over-investment, researchers typically integrate other resilience enhancement measures with planning model. Early resilience-oriented planning model mainly focuses on integrating single resilience enhancement measure like line hardening with planning [19]. At present, many works tend to involve more resilience enhancement resources into planning model to further mitigate the conservatism of planning model. Both [20,21] consider the joint of generation and transmission expansion planning, with the difference being that [20] also optimizes micro grid penetration, while [21] further considers FACTS devices planning. [22] taking into account the optimal transmission switching and differential load-shedding measures, simultaneously optimizes the transmission and substation expansion plan to resist HILP events. Compared with transmission expansion planning, distribution expansion planning models often incorporate a broader range of resilience enhancement measures. [23]– [24] combine distribution expansion planning with hardening, while [23] also optimizes tie-line installation and [24] takes network reconfiguration into account. [25–28] focus on distribution network hardening model. Among them, [25–27] also plan the installation of distributed generation, [25,26] embed the microgrid formation to hardening model, [26,27] further considers the deployment of switches and topology reconfiguration and [27,28] allocate mobile emergency generators or energy storage system to enhance resilience. It can be seen that integrating planning with various source-grid-load measures is the prevailing trend, and for resilience-oriented planning considering typhoon disasters, integration with hardening is a common feature of many works. However, the hardening models in these studies are overly simplified, assuming that hardened lines cannot fail and all lines share the same hardening level, which fail to fully reflect the characteristics of transmission planning problem. Additionally, the resilience-oriented coordinated planning of OWF and transmission network has not been studied yet.

1.3. Research gap

- For existing wind farm output uncertainty models, on one hand, they ignore the significantly increased risk of wind turbine failures under TDS, underestimating the impact of typhoons on wind farm output. On the other, they neglect the differences in wind farm output uncertainty between typhoons and normal scenarios, making them less suitable for planning problem which require consideration of both normal and typhoon scenarios. For grid fault uncertainty models, on one hand, they often focus on a single type of fault under TDS, such as high probability faults or high loss faults, which correspondingly underestimate or overestimate the impact of typhoons. On the other, although the state-of-art researches have begun to model the uncertainty of component failure rates under TDS, there is still a lack of attention to the probability distribution uncertainty of fault scenarios under TDS.
- Lack of ROWF&TNIP that coordinates economy and resilience requirements under both NOS and TDS. Existing resilience-oriented transmission planning considering typhoon disasters have two limitations. On one hand, they neglect the integration of OWF, which may play an important role in resilience enhancement. On the other, more importantly, they often merely focus on resilience requirement under TDS, failing to take into account the economy requirement such as wind power absorption under NOS. This may not only lead to overly conservative planning schemes, but also contradict the actual needs of transmission planning in real life. Thus, a resilience-oriented planning model encompassing both NOS and TDS is crucial. While some hardening models aim to address this gap [26,28], to our knowledge, no transmission planning model has yet incorporated this crucial issue.
- Lack of a detailed and cost-effective hardening model and a proper method to integrate hardening with planning. Hardening model has not been refined in line with the features of transmission planning problem. Firstly, transmission lines span vast distances, and different sections of one transmission line may experience different wind speeds under TDS. However, existing models often apply a uniform hardening level to one transmission line, neglecting the variability in typhoon wind speeds across different line sections. Secondly, many hardening models assume that hardened lines are completely impervious to failure. However, in reality, hardening reduces the failure rate but does not guarantee immunity from damage. While some hardening models avoid this oversimplification, they have not jointly modeled hardening and expansion planning; otherwise, it would be challenging to design the solution procedures for the whole model. This modeling approach may hinder the comparative analysis of cost-effectiveness of planning and hardening measures, leading to overlapping investments.

Given the above, this paper proposes a R&E coordinated OWF&TNIP model considering typhoon. Main contributions are as follows:

- Develop a multi-scenario distributionally robust uncertainty model for OWF output and grid fault. For OWF output uncertainty, a CVaR-based multi-scenario budget uncertainty set is built, of which the robust budget uncertainty set is employed to address the turbine output uncertainty resulted by wind speed forecasting error, while CVaR is used to quantify turbine failures uncertainty considering turbine failure rate. This budget uncertainty set is extended to multi-scenario form to capture the differences in OWF output uncertainty between TDS and NOS. For gird fault uncertainty, a 1-norm grid fault uncertainty set is constructed to depict the uncertain probability distribution of four types of grid faults: high-probability faults, high-loss faults, cascading faults under TDS and fault-free state under NOS.
- Propose a ROWF&TNIP model coordinating economy and resilience requirements under both NOS and TDS. As potential resilience enhancement resources, OWF is jointly planned with transmission network. Based on the above uncertainty sets. The proposed ROWF&TNIP exhibits a tri-level multi-scenario distributionally robust optimization structure. With the worst-case expected load-shedding cost under TDS as resilience index, the planning and expected generation cost under TDS and NOS as economic index, the ROWF&TNIP coordinates resilience and economy with the worst-case of OWF outputs and grid faults probability distribution under NOS and TDS. Short-term measures like preventive unit commitment, differential load-shedding and differential hardening are embedded into the planning model to mitigate its conservatism.
- Design a differential hardening model and integrate it with ROWF&TNIP to prevent excessive investment. First, transmission lines are segmented into multiple sections based on varying typhoon wind speeds, and each section undergoes hardening at different levels. Subsequently, we devise an appropriate process to integrate differential hardening and ROWF&TNIP, guaranteeing that hardening only reduce the probability of fault scenarios, and simultaneously obtaining the hardening and planning outcome. Lastly, a cost-efficiency sensitivity analysis is performed across various hardening strategies.

The rest of the paper is organized as follows: Section II demonstrates the uncertainty model for OWF output and grid fault. Section III introduces the mathematical formulation of the proposed ROWF&TNIP model. Section IV describes the solution algorithm. Section V presents the case study results and Section VI summarizes the conclusions.

2. Uncertainty model for OWF output and grid fault

2.1. Uncertainty model overview

Fig. 1 presents the framework of the comprehensive multi-scenario distributionally robust uncertainty model for OWF output and grid fault under both NOS and TDS. This uncertainty model consists of a CVaR-based multi-scenario robust budget uncertainty set for OWF output and a 1-norm distributionally robust uncertainty set for grid fault probability distribution. This setting is partly due to the suitability of robust and distributionally robust models for optimization problems considering extreme scenarios like typhoon disasters, and partly due to the different available data and theoretical foundations of OWF output and grid fault.

For OWF output uncertainty model, we consider two sources of uncertainty in OWF output: one is the uncertain individual turbine output resulted by wind speed forecasting error and the other is the uncertain turbine failures considering turbine failure rate. Given that the fluctuation range of turbine output can be obtained according to the historical wind speed forecasting error data, the robust budget uncertainty set is employed to depict the uncertain turbine output range. Considering that the turbine failure rate model has already been studied, we utilize the CVaR to quantify the uncertain number of failed turbines in a wind farm. Ultimately, the aggregate uncertain outputs from the functioning turbines in the OWF are designated as the OWF output uncertainty model. Furthermore, noticing that the wind speed forecasting error and turbine failure rate might exhibit significantly difference between NOS and TDS, we extend the CVaR-based budget uncertainty set to the multi-scenario form to represent the difference in OWF output uncertainty between normal and typhoon scenarios.

For grid fault uncertainty model, we notice that: a) most of the time, power system operates in a fault-free state under NOS, and b) power system confronts at least three types of fault risk: higher line failure rate near typhoon center, serious losses in heavily loaded areas caused by N-k faults, and cascading failures due to power flow transfers triggered by initial typhoon-induced faults. Based on these observations, we categorize grid faults under TDS and NOS into four types: high-probability faults, high-loss faults, and cascading faults under TDS and fault-free

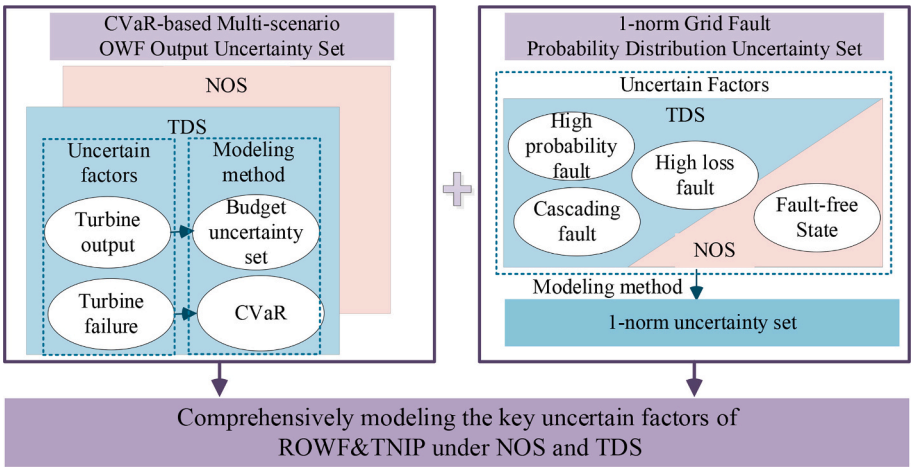

Fig. 1. The framework of the OWF output and grid fault uncertainty set.

state under NOS. Moreover, considering the actual probability of these fault scenarios are hard to be accurately predicted but the theoretical probability can be determined based on existing component failure rate model, we utilize 1-norm uncertainty set widely used in distributionally robust optimization to characterize the uncertain deviation between actual and theoretical probability distribution of the four types grid fault scenarios.

2.2. OWF output uncertainty model

We take four steps to construct a multi-scenario CVaR-based budget uncertainty set to capture the uncertain OWF output under NOS and TDS. Specifically, steps 1 and 2 develop an individual turbine output uncertainty model, while step 3 models the uncertain failed turbines count. Finally, step 4 integrates these two models to form a comprehensive OWF output uncertainty model.

Step 1: calculation of theoretical turbine output under NOS and TDS. The characteristics of turbine output vary significantly under TDS and NOS. Fig. 2(a) illustrates a typical daily turbine output ratio curve for a wind farm located in East China. The theoretical turbine output under NOS is derived from this curve. Within a typhoon wind field, wind speed distribution demonstrates a bimodal characteristic: the wind speed increases from 0 to its maximum value from the typhoon eye to maximum wind speed radius, and begins to decline once the maximum wind speed radius is surpassed. Given a scenario where a typhoon starts approaching a wind farm at t0, with the typhoon eye and maximum wind speed radius gradually reaching and moving away from the turbine, the turbine output ratio exhibit variations as depicted in Fig. 2(b). The detailed description of typhoon stages corresponding to each time interval in Fig. 2(b) is presented in Appendix A. It's important to note that turbine output will be zero when the wind speed falls below the cut-in threshold or exceeds the cut-out threshold. To quantify the theoretical turbine output, the widely used BATTs model is used to simulate the typhoon wind field dynamic process [29], and the turbine output under forecasted wind speed w_t is calculated by (1) [30].

$$p_{wt}^{TH} = \begin{cases} 0, w_t \leqslant w_{ci}, w_{co} \leqslant w_t \\ p_w^R\left(A + Bw_t + Cw_t^2\right), w_{ci} \leqslant w_t \leqslant w_R \\ p_w^R, w_R \leqslant w_t \leqslant w_{co} \end{cases} \tag{1}$$

where p_{wt}^{TH}, p_w^R are theoretical and rated outputs of turbine w at time t, w_{ci}, w_{co}, w_R are cut in, cut out and rated wind speed , A,B,C are the wind-power conversion model coefficients.

Step 2: uncertainty set of individual turbine output. We assume the actual turbine output p_{wts} at time t under scenario s fluctuates within a range related to wind speed forecasting error, which can be described by (2).

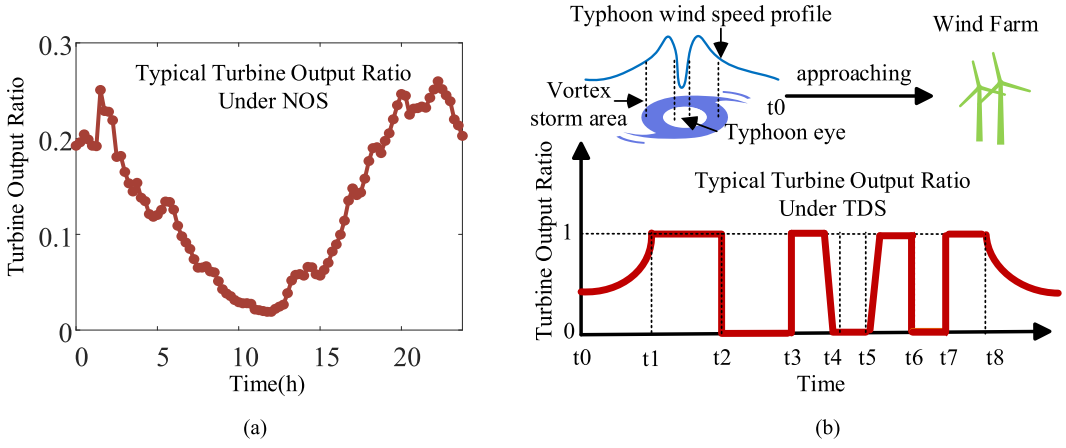

Fig. 2. Typical turbine output ratio under NOS and TDS.

$$\Omega_{WTO}=\left\{\begin{array}{l} k_2^T p_{wts}^{TH}\leqslant p_{wts}\leqslant k_1^T p_{wts}^{TH}, s\in S_T \\ k_2^N p_{wts}^{TH}\leqslant p_{wts}\leqslant k_1^N p_{wts}^{TH}, s\in S_N \\ \sum\limits_{s\in S,w\in W,t\in T}\left|\dfrac{p_{wts}-p_{wts}^{TH}}{\Delta_{wst}^{TH}}\right|\leqslant \Gamma \\ k_1^T,k_1^N\in[1,\infty], k_2^T,k_2^N\in[0,1] \end{array}\right\} \tag{2}$$

where Ω_{WTO} is the uncertainty set of individual turbine output, S_T, S_N are scenario sets of TDS and NOS. k_1^T, k_2^T and k_1^N, k_2^N are scaling coefficients representing upper and lower deviation of actual turbine output under TDS and NOS, and they are not linearly related to wind speed forecasting error. Take k_1^T for example, its value is determined by (3). Δ_{wst}^{TH} is the sum of the possible deviation of p_{wts} and p_{wts}^{TH}, for example, under TDS, $\Delta_{wst}^{TH}=\left(k_1^T-1\right)p_{wts}^{TH}+\left(1-k_2^T\right)p_{wts}^{TH}$. Γ is the budget of uncertainty set, which adjusts the conservatism by constraining the total deviation degree of p_{wts} and p_{wts}^{TH}.

$$\left\{\begin{array}{l} k_1^T=\left\{\begin{array}{l} 0, \widehat{w}_t\leqslant w_{ci}, \widehat{w}_t\geqslant w_R \\ \dfrac{(A+B\widehat{w}_t+C\widehat{w}_t^2)}{(A+Bw_t+Cw_t^2)}, w_{ci}\leqslant\widehat{w}_t\leqslant w_R \end{array}\right. \\ \widehat{w}_t=(1+k_E)w_t, k_E>0 \end{array}\right. \tag{3}$$

where k_E is wind speed forecasting error under TDS, $\widehat{w}_t$ is actual wind speed, for lower limit scaling coefficients like k_2^T, $\widehat{w}_t=\left(1\text{-}k_E^T\right)w_t$, the difference between TDS and NOS lies in different k_E.

Step3: turbine failure risk model. Contrary to many studies that employ mathematical expectation to characterize the turbine failure risk, we recognize that expectation is inadequate to describe the tail risk of typhoon disasters. Given the significance of planners' risk tolerance in shaping planning outcomes, we incorporate the classical risk management approach CVaR to quantify the failure risk of turbines under NOS and TDS. The CVaR can be defined by (4) [31].

$$\left\{\begin{array}{l} N_{CVaR}=E(N|N\geqslant N_{VaR})=\dfrac{1}{1-\beta}\displaystyle\int_{N_{VaR}}^{N_{max}}N\rho(N)\mathrm{d}N \\ N_{VaR}=min\{n|\mathrm{P}(N\leqslant n)\geqslant\beta\} \end{array}\right. \tag{4}$$

where $E(\bullet)$ represents mathematical expectation, ρ, P are probability density function and cumulative probability distribution function of variable N, β is confidence level which belongs to $(0,1)$, N_{VaR} is value at risk (VaR) of N. Given the discrete distribution of turbine failure, the CVaR of failed turbines under scenario s N_{CVaR}^s can be described by (5).

$$\left\{\begin{array}{l} N_{CVaR}^s=\dfrac{1}{1-\beta}\displaystyle\sum_{m=N_{VaR}}^{N_W}\left[N_f^s p\left(N_f^s=m\right)\right] \\ N_{VaR}^s=min\left\{n\left|\left[\displaystyle\sum_{m=0}^{n}p\left(N_f^s=m\right)\right]\geqslant\beta\right.\right\} \end{array}\right. \tag{5}$$

where N_f^s is number of failed turbines under scenario s, N_W is the total number of turbines in wind farm W. $p\left(N_f^s=m\right)$ is probability of m failed turbines, which can determined by (6).

$$\left\{\begin{array}{l} p\left(N_f=m\right)=C(N_W,m)\left(\lambda_w^s\right)^m\left(1-\left(\lambda_w^s\right)\right)^{N_W-m} \\ \lambda_w^s=\left\{\begin{array}{l} \lambda_w^{norm}, w_t\leqslant w_R \\ \left[1+\left(\dfrac{1}{\lambda_w^{norm}}-1\right)exp(-\gamma(w_t-w_R))\right]^{-1}, w_R\leqslant w_t\leqslant w_{co} \end{array}\right. \\ C(N_W,m)=\dfrac{N_W!}{m!(N_W-m)!} \end{array}\right. \tag{6}$$

where $\lambda_w^s, \lambda_w^{norm}$ are failure rate of turbine w under scenario s and normal conditions.

Step 4: OWF output uncertainty set. Given that in practical, it would be difficult for transmission system operators to obtain the output of each turbine output in a large wind farm, it is assumed that all turbines in a wind farm share the same output. Since OWF output is the total output of turbines operating normally, and the difference between TDS and NOS mainly lies in the wind speed forecasting error and CVaR of failed turbines, the OWF output uncertainty set Ω_{WFO} is denoted as (7).

$$\Omega_{WFO}=\left\{p_{Wst}\left|\begin{array}{l} k_2^T p_{wts}^{TH}\leqslant p_{wts}\leqslant k_1^T p_{wts}^{TH}, s\in S_T \\ k_2^N p_{wts}^{TH}\leqslant p_{wts}\leqslant k_1^N p_{wts}^{TH}, s\in S_N \\ \displaystyle\sum_{s\in S,w\in W,t\in T}\left|\dfrac{p_{wts}-p_{wts}^{TH}}{\Delta_{wst}^{TH}}\right|\leqslant\Gamma \\ p_{Wst}=(N_W-N_{CVaR}^s)p_{wst} \\ p_{Wst}^{TH}=(N_W-N_{CVaR}^s)p_{wst}^{TH} \end{array}\right.\right\} \tag{7}$$

where p_{Wst}, p_{Wst}^{TH} are actual and theoretical outputs of wind farm W at time t under scenario s. The whole process of constructing OWF output uncertainty set is shown in Fig. 3.

2.3. Grid fault uncertainty model

We take four steps to develop the 1-norm grid fault uncertainty set which captures the uncertain probability distribution of four types of grid fault.

Step 1: search for high-probability faults. (8) is adopted to calculate the line failure rate under TDS [32].

$$\left\{\begin{array}{l} \lambda_{lt}(w_t)=\left\{\begin{array}{l} \lambda_l^{norm}, w_t\leqslant w_r \\ \lambda_l^{norm}+exp\left[\left(\dfrac{0.6931(w_t-w_r)}{w_r}\right]-1\right)\right], w_r<w_t<2w_r \\ 1, w_t\geqslant 2w_r \end{array}\right. \\ \lambda_l^w=1-exp\left[-\displaystyle\int_{t_0}^{t_e}\lambda_{lt}(w_t)dt\right] \end{array}\right. \tag{8}$$

where w_r is wind speed threshold, λ_l^{norm} is the failure rate of line l under NOS. $\lambda_{lt}(w_t), \lambda_l^w$ are the failure rate of line l at wind speed w_t and throughout TDS.

All lines are sorted in descending order based on their failure rates, and the lines with higher failure rate are combined to form a set of high probability N-k faults. Take N-1 and N-2 for example, the N-k faults probability can be calculated by (9) [33].

$$\left\{\begin{array}{l} p(Z_1)=\lambda_l^w-\displaystyle\sum_{i=1}^{L}v_{li}+\frac{1}{2}\sum_{i=1}^{L}\sum_{j=1}^{L}v_{lij}-\frac{1}{6}\sum_{i=1}^{L}\sum_{j=1}^{L}\sum_{h=1}^{L}v_{lijh}+\cdots \\ \qquad\qquad i\neq l \qquad\qquad i\neq l\quad j\neq l,i \qquad\qquad i\neq l\quad j\neq l,i\quad h\neq l,i,j \\ p(Z_2)=v_{li}-\displaystyle\sum_{j=1}^{L}v_{lij}+\frac{1}{2}\sum_{j=1}^{L}\sum_{h=1}^{L}v_{lijh}+\cdots \\ \qquad\qquad j\neq l,i \qquad\qquad j\neq l,i\quad h\neq l,i,j \\ v_{li}=\lambda_l^w\lambda_i^w, v_{lij}=\lambda_l^w\lambda_i^w, v_{lijh}=\lambda_l^w\lambda_i^w\lambda_j^w\lambda_h^w \end{array}\right. \tag{9}$$

where Z_1 represents only line l fails, Z_2 represents only lines l, i fail, $p(Z_1), p(Z_2)$ are their probabilities.

Step 2: high-loss faults. Based on classical attack-defense-attack model [34], the N-k faults resulting in serious load-shedding are

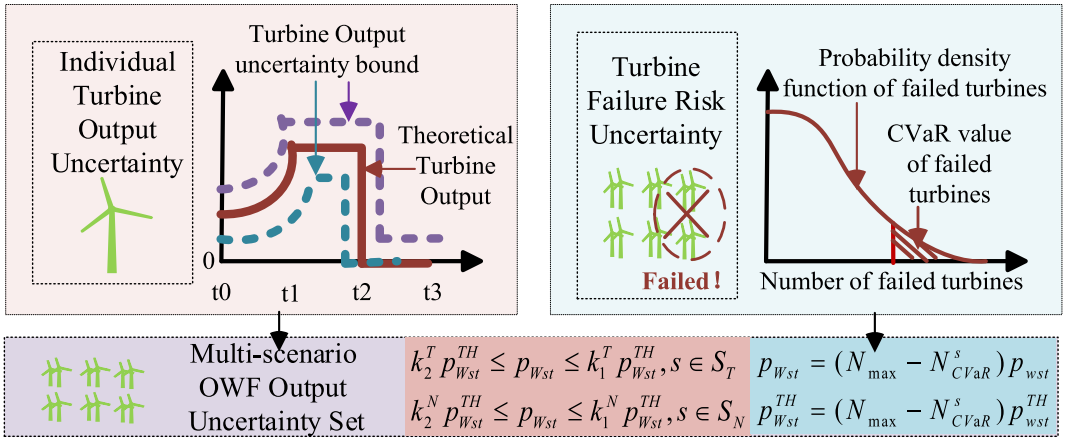

Fig. 3. Construction process of OWF output uncertainty set.

searched by (10) to construct the high-loss faults set, and the corresponding probabilities are calculated by (9).

$$\min_{p_{lt},p_{gt},\Delta D_{bt}\in\mathscr{G}_1} \max_{z\in\Omega_f} \min_{p_{lt},p_{gt},\Delta D_{bt}\in\mathscr{G}_2} f\left(\Delta D_{bt}, p_{gt}, p_{lt}\right)$$
$$\Omega_f = \left\{ \sum_{l\in L} z_l \geqslant N_L - K_{max} \right\} \tag{10}$$

where $p_{gt}, p_{lt}, \Delta D_{bt}$ are output of generator g, power flow of line l and load-shedding at bus b at time t, $\mathscr{G}_1$, $\mathscr{G}_2$ are feasible zones of decision variables before and after faults, Ω_f is N-k faults set, z_l is fault state variable of line l, $z_l = 1/0$ represents normal/fault state. N_L is total number of lines, $K_{\max}$ is maximum number of failed lines.

Step 3: cascading faults. Firstly, construct an initial fault set which covers the lines with high failure rate during TDS and select one line from the set to trip out as the initial fault. Secondly, the fault chain search is carried out based on (11) and the line with the maximum failure rate caused by overload is selected as the subsequent disconnected line, and the search of one fault chain is ended if N-k criteria is satisfied.

$$\lambda_l^C = \begin{cases} \lambda_l^{norm}, p_{lt} \leqslant p_l^R \\ \lambda_l^{norm} + \dfrac{\left(1-\lambda_l^{norm}\right)\left(p_{lt}-p_l^R\right)}{p_{lt}-p_l^{max}} \Bigg), p_l^R \leqslant p_{lt} < p_l^{max} \\ 1, p_{lt} \geqslant p_l^{max} \end{cases} \tag{11}$$

where λ_l^c is failure rate of line l under cascading fault chain c. $p_l^R, p_l^{\max}$ are rated and limit power of line l.

Considering that both wind speed and cascading fault have an impact of the line failure rate, and assuming that the λ_l^w, λ_l^C are independent, the comprehensive failure rate λ_l^F of line l can be obtained by (12), and the probability of each N-k cascading fault chain can be determined by (9).

$$\begin{cases} \lambda_l^C = \dfrac{\sum_{\forall c\in C} \lambda_l^c}{N_c} \\ \lambda_l^F = \lambda_l^w + \lambda_l^C - \lambda_l^w \lambda_l^C \end{cases} \tag{12}$$

where C is initial fault set including N_c high risk lines, λ_l^C is failure rate of line l under all cascading fault chains.

Step 4: 1-norm grid fault uncertainty set. Assuming that N_1, N_2, N_3 fault scenarios are searched for the former three fault types, respectively, combined with the fault-free scenario under NOS, there are a total of $N_c = 1 + N_1 + N_2 + N_3$ scenarios under the fault scenario set that considers NOS and TDS. The sum of probabilities for these scenarios equals 1, where the sum of probabilities for the $N_c - 1$ fault scenarios under TDS is equal to the proportion of typhoon days in a year. The probability of each fault scenario is calculated by (9) and then normalized to ensure that the sum of the probability distribution of all fault scenarios equal 1. Considering the deviations in the actual probability distribution of these fault scenarios from the theoretical calculation, we adopt the 1-norm uncertainty set (13) to characterize such deviations based on the idea of distributionally robust optimization.

$$\Omega_{GF} = \left\{ p_s(Z_s) \left| \begin{array}{l} \sum_{s\in S_T} |p_s(Z_s) - p_0(Z_s)| \leqslant \Psi \\ \partial_1 p_0(Z_s) \leqslant p_s(Z_s) \leqslant \partial_2 p_0(Z_s), s \in S_T \\ \sum_{s\in S} p_s(Z_s) = 1 \\ S = S_T \cup S_N \\ \sum_{s\in S_T} p_s(Z_s) = \dfrac{T_D}{365} \\ p_s(Z_s) \geqslant 0 s \in S \end{array} \right. \right\} \tag{13}$$

where Ω_{GF} is the 1-norm grid fault uncertainty set, $p_s(Z_s), p_0(Z_s)$ are the actual and normalized theoretical probability of fault scenario Z_s, $\Psi, \partial_1, \partial_2$ are parameters limiting the total and individual probability deviations of fault scenario Z_s under TDS. In the case of a large sample data size, the Ψ can be determined using an empirical formula. However, for HILP event, relying on engineering experience is a viable option, and the value of these three parameters can adjust the conservatism of the model. T_D is average annual typhoon days. To facilitate the subsequent solution of the ROWF&TNIP model, the absolute value expression in the set is equivalently transformed to (14) by introducing $p_k(Z_s)$, and the structure of the uncertainty set is illustrated in Fig. 4.

$$\sum_{s\in S_T} |p_s(Z_s) - p_0(Z_s)| \leqslant \Psi \Leftrightarrow \left\{ \begin{array}{l} \sum_{s\in S_T} p_k(Z_s) \leqslant \psi \\ p_k(Z_s) \geqslant p_s(Z_s) - p_0(Z_s), s \in S_T \\ p_k(Z_s) \geqslant p_0(Z_s) - p_s(Z_s) s \in S_T \\ \dfrac{\sum_{s\in S_T \cup S_N} p_k(Z_s) = 1}{p_k(Z_s) \geqslant 0, s \in S} \end{array} \right. \tag{14}$$

2.4. Connection between the uncertainty model and ROWF&TNIP model

It can be seen that the proposed uncertainty sets $\Omega_{WFO}, \Omega_{GF}$ are essentially a series of constrains of wind farm outputs p_{Wst} and actual fault probability $p_s(Z_s)$, and these constraints are the constraints of the middle level of the tri-level ROWF&TNIP model. Besides, $p_{Wst}, p_s(Z_s)$ are reflected in the constraints and objective function of the ROWF&TNIP

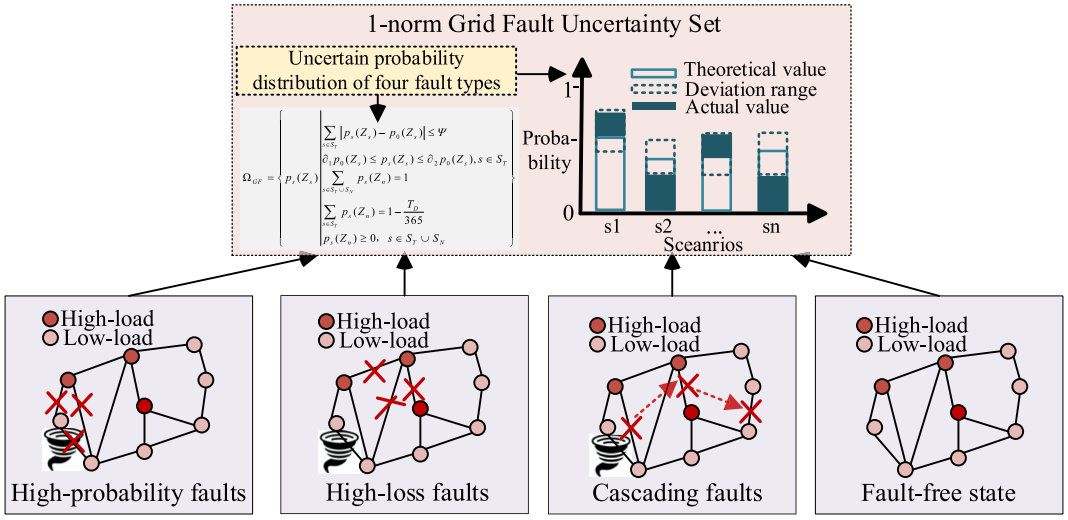

Fig. 4. Structure of grid fault uncertainty set.

model, respectively. A detailed presentation of how $\Omega_{WFO}, \Omega_{GF}$ are integrated into the ROWF&TNIP model is presented in the subsequent section.

3. Multi-scenario distributionally robust ROWF&TNIP model

3.1. Model overview

The multi-scenario distributionally robust ROWF&TNIP model follows a tri-level min-max-min framework, and the decisions made in each level are outlined as follows:

a) The upper-level problem minimizes the total costs of three kinds of preventive measures: OWF and transmission expansion planning, differential hardening and preventive unit commitment.

b) Obtaining the prevention schemes from upper-level, the middle-level problem searches in the uncertainty set for the worst-case of OWF outputs and grid fault probability distribution, which cause the max expected operational cost under NOS and TDS.

c) Given the prevention results and the worst scenarios from upper and middle level, the lower-level problem minimizes the expected cost of generation redispatch and differential load-shedding under NOS and TDS to coordinate resilience and economy.

The framework of the proposed ROWF&TNIP model is shown in Fig. 5.

3.2. Objective function

$$\min_{\substack{x_l, x_W, u^S_{gst}\\ u^D_{gst}, u^o_{gst}\in G}} \left\{ f_1 + \max_{\substack{p_s(Z_s)\in\hat{\Omega}_{GF}\\ p_{Wst}\in\Omega_{WFO}}} \left[\sum_{s\in S} \left(p_s(Z_s) \min_{\substack{p_{gst}, p_{lst}, p_{rwst}\\ p_{r1st}, p_{r2st}\in H}} f_2 \right) \right] \right\} \tag{15}$$

$$f_1 = \sum_{l\in L_c} C^L_l x_l + \sum_{W\in L_W} C^{OWF}_W x_W + C^H + \sum_{s\in S}\sum_{t\in T}\sum_{g\in G} \left(C^S_g u^S_{gst} + C^D_g u^D_{gst} \right) \tag{16}$$

$$f_2 = \sum_{s\in S}\sum_{t\in T} \left[\sum_{g\in G} C^G_g p_{gst} + \sum_{r_w\in L_W} C^{WC}_{r_w} p_{r_w st} + \sum_{r_1, r_2\in B} \left(C^{LS}_{r_1} p_{r_1 st} + C^{LS}_{r_2} p_{r_2 st} \right) \right] \tag{17}$$

where f_1, f_2 objective function of upper and lower level problem, x_l, x_W, $u^S_{gst}, u^D_{gst}, u^o_{gst}$ are binary decision variables of line and OWF investment, generator start, shut down and operation state, and 1 means these measures are taken, 0 otherwise. $C^L_l, C^{OWF}_W, C^S_g, C^D_g$ are the corresponding costs. C^H is the cost of differential hardening, which will be introduced in detail in the D model part. $p_{gst}, p_{lst}, p_{r_w st}, p_{r_1 st}, p_{r_2 st}$ are generator output, power flow, wind power curtailment, important and normal load shedding at time t under scenario s. $C^G_g, C^{WC}_{r_w}, C^{LS}_{r_1}, C^{LS}_{r_2}$ are corresponding costs. B, G, L_W, L_c, L_e are sets of buses, generators, OWF, candidate and existing lines. $\mathscr{G}, \mathscr{H}$ are feasible regions of upper and lower-level problem. $\widehat{\Omega}_{GF}, \Omega_{WFO}$ are feasible regions of middle-level problem.

In (15), we take the expected load-shedding cost under the worst-case grid fault probability distribution under TDS searched by the middle level problem as the resilience index, which can be represented as (18). The economic index is the other cost in (15). Thus, the system's resilience performance under TDS and its economic performance under both TDS and NOS can be simultaneously considered.

$$\max_{\substack{p_s(Z_S)\in\hat{\Omega}_{GF}\\ p_{Wst}\in\Omega_{WFO}}} \left[\sum_{s\in S_T} \left(p_s(Z_s) \min_{\substack{p_{gst}, p_{lst}, p_{rwst}\\ p_{r1st}, p_{r2st}\in H}} \sum_{s\in S_T}\sum_{t\in T} \left[\sum_{r_1, r_2\in B} \left(C^{LS}_{r_1} p_{r_1 st} + C^{LS}_{r_2} p_{r_2 st} \right) \right] \right) \right] \tag{18}$$

3.3. Upper level constraints

(1) Budget constraints

$$\begin{cases} \sum_{l\in L_c} C^L_l x_l \leqslant \prod_L \\ \sum_{W\in L_W} C^{OWF}_W x_W \leqslant \prod_W \end{cases} \tag{19}$$

where $\prod_L, \prod_W$ are lines and OWF investment budgets.

(2) Preventive unit commitment constraints

$$\begin{cases} u^o_{gs}(t-1) - u^o_{gs}t + u^o_{gs}k \leqslant 1 \forall t \in T, 1 \leqslant k - (t-1) \leqslant T^D_g \\ -u^o_{gs}(t-1) + u^o_{gs}t - u^o_{gs}k \leqslant 0 \forall t \in T, 1 \leqslant k - (t-1) \leqslant T^S_g \\ -u^o_{gs}(t-1) + u^o_{gs}t - u^S_{gs}t \leqslant 0, \forall g \in G, \forall s \in S, \forall t \in T \\ -u^o_{gs}(t-1) + u^o_{gs}t - u^D_{gs}t \leqslant 0 \forall g \in G, \forall s \in S, \forall t \in T \\ u^o_{g(s-1)}t = u^o_{gst} \forall s \in S_T \end{cases} \tag{20}$$

where T^D_g, T^S_g are minimum continuous shutdown/ startup time of the generator g. $u^o_{g(s-1)}t = u^o_{gst}$ $\forall s \in S_T$ has two implications: on one hand, we employ different preventive unit commitment strategies to tackle TDS and NOS; on the other hand, we only optimize one preventive unit

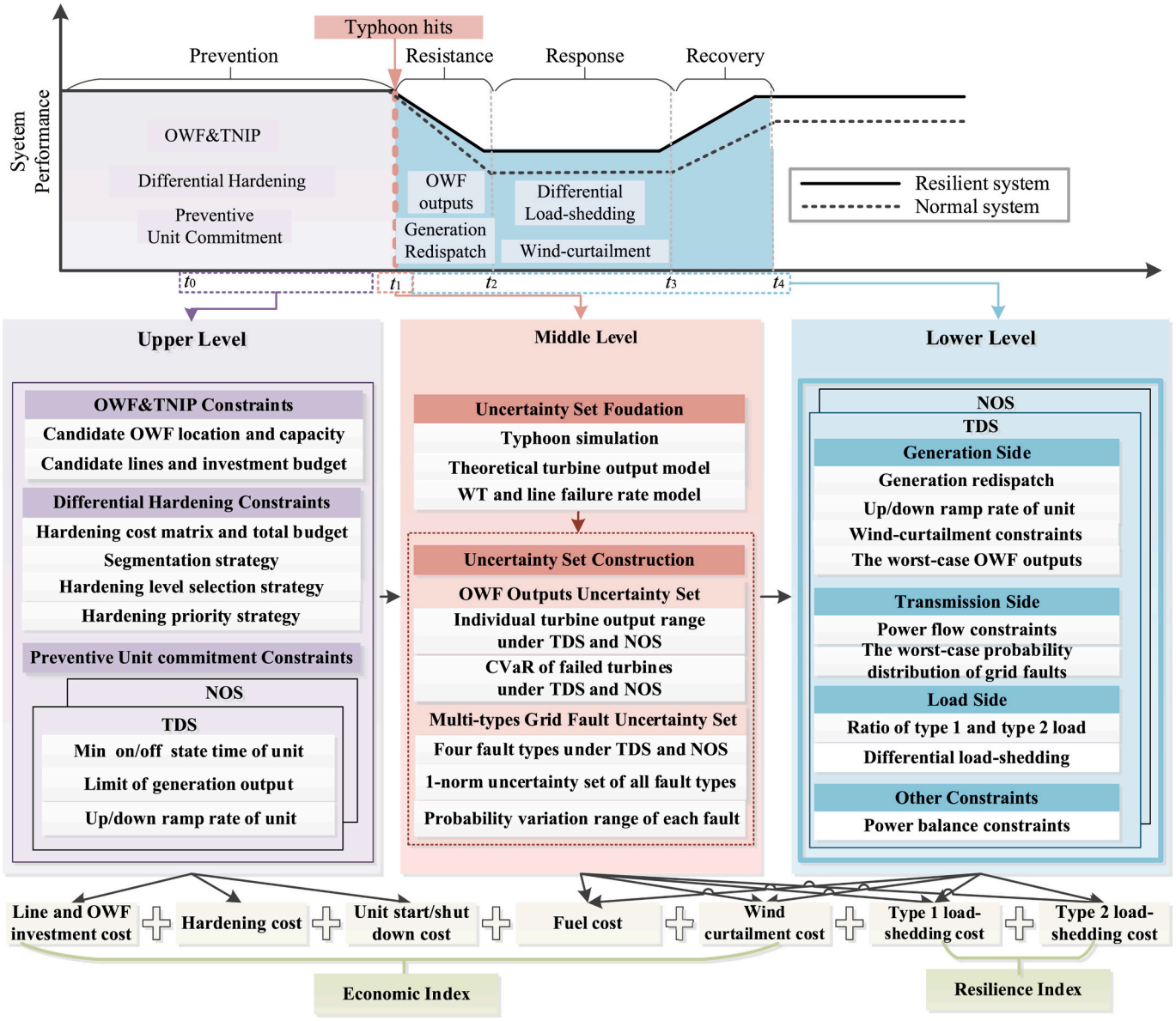

Fig. 5. The framework of the proposed ROWF&TNIP model.

commitment strategy for all faults scenarios under TDS, given that in practical, dispatchers can only utilize a single preventive unit commitment strategy to resist all potential faults under a given TDS. (19)–(20) is the feasible region Gof upper-level problem.

(3) Differential hardening model.

The proposed differential hardening model aims to harden different segments of a transmission line with varying degrees based on the difference in wind speed along each segment during TDS. We adopt a three-step approach to construct the differential hardening model.

Step 1: Establish a set of lines for hardening. Lines included in the fault uncertainty set are eligible for hardening, however, considering the hardening cost budget constraint, we select $\prod_H$ lines with the higher failure rates to constitute the set of lines for hardening.

Step 2: Design a differential hardening segment division strategy and calculate differential hardening costs. Following international practices, the wind speed range for typhoon intensity levels is 3–5 m/s. In practice, one hardening level be applicable to one or more typhoon intensity levels. Thus, designing the segment division strategy involves constructing a piecewise function (21) that characterizes different wind speed intervals and their corresponding hardening levels. The calculation of differential hardening costs requires a piecewise function (22) to determine the costs associated with different hardening levels. The total hardening cost is calculated by (23).

$$\begin{cases} h_e(\widehat{w}_e) = \begin{cases} h_a^{Level}, w_1^R \leqslant \widehat{w}_e < w_2^R \\ h_b^{Level}, w_2^R \leqslant \widehat{w}_e < w_3^R \\ h_c^{Level}, w_3^R \leqslant \widehat{w}_e < w_4^R \\ \cdots \end{cases} \\ \widehat{w}_e = \underset{t \in T}{max}(w_{et}) \end{cases} \tag{21}$$

$$C_e^H(h_e) = \begin{cases} C_a^H, h_e = h_a^{Level} \\ C_b^H, h_e = h_b^{Level} \\ C_c^H, h_e = h_c^{Level} \\ \cdots \end{cases} \tag{22}$$

$$\begin{cases} C^H = \sum_{l\in L_h} C_l^H \\ C_l^H = \sum_{e\in E_l} \left[C_e^H(h_e) h_e(\widehat{w}_e) \right] \end{cases} \tag{23}$$

where $h_e(\widehat{w}_e), C_e^H(h_e)$ are piecewise functions of segment division strategy and hardening cost. $w_1^R \sim w_4^R$ are threshold of each wind speed interval, $h_a^{Level} \sim h_c^{Level}$ are hardening levels corresponding to each wind speed interval, and $C_a^H \sim C_b^H$ are the corresponding hardening costs. The differences in the values of these three sets of parameters reflect different hardening strategies. $\widehat{w}_e$ is the maximum wind speed of segment e during typhoon, C_l^H is the hardening cost of line l, L_h, E_l are sets of lines for hardening and all segments of line l.

Step 3: Update the fault uncertainty set after hardening and integrate the differential hardening model with ROWF&TNIP. Unlike previous works that assume hardened lines are invulnerable during TDS, we adopt a more realistic assumption that hardening merely reduces the failure rate. Consequently, the line failure rate is updated after hardening according to (24). Based on this, the probability of fault scenarios and the fault uncertainty set are also updated using (9) and (25). Given that hardening is more cost-effective than planning, to integrate the differential hardening and ROWF&TNIP models, differential hardening is firstly utilized to harden the high-risk lines. After updating the fault uncertainty set, the planning process is conducted to avoid excessive investment. Fig. 6 shows the modeling process of the differential hardening.

$$\widehat{\lambda}_l^w = 1 - \prod_{e\in E_l} \left(1 - \lambda_e^w(h_e)\right) \tag{24}$$

$$\begin{cases} \sum_{s\in S_T} |p_s(Z_s) - \widehat{p}_0(Z_s)| \leqslant \Psi \\ \partial_1 \widehat{p}_0(Z_s) \leqslant p_s(Z_s) \leqslant \partial_2 \widehat{p}_0(Z_s), s \in S_T \end{cases} \tag{25}$$

where $\lambda_e^w(h_e)$ is the failure rate of segment e of line l with hardening level h_e which enhances the wind speed threshold W_r in line failure rate model (8). $\widehat{\lambda}_l^w$ is the failure rate of hardened line l, $\widehat{p}_0(Z_s)$ is the updated theoretical fault probability after hardening.

3.4. Middle level constraints

The middle level problem is a maximization problem that searches for the OWF output p_{Wst} and actual grid fault probability distribution $p_s(Z_s)$ in the uncertainty set $\Omega_{WFO}, \widehat{\Omega}_{GF}$, to maximize the expected operation cost. Therefore, the middle level constraints are the uncertainty set $\Omega_{WFO}, \widehat{\Omega}_{GF}$. Given that the middle level searches for the worst-case $p_s(Z_s)$ only after the hardening measure is conducted in the upper level, the middle level problem should adopt the updated grid fault uncertainty set $\widehat{\Omega}_{GF}$ after hardening, rather than the original grid fault uncertainty set Ω_{GF} as (13), that is, the theoretical fault probability is $\widehat{p}_0(Z_s)$, rather than $p_0(Z_s)$. The $\Omega_{WFO}, \widehat{\Omega}_{GF}$ adopted in middle level are presented as (26)–(27).

$$\Omega_{WFO} = \left\{ p_{Wst} \;\middle|\; \begin{array}{l} k_2^T p_{Wst}^{TH} \leqslant p_{Wst} \leqslant k_1^T p_{Wst}^{TH}, s \in S_T \\ k_2^N p_{Wst}^{TH} \leqslant p_{Wst} \leqslant k_1^N p_{Wst}^{TH}, s \in S_N \\ p_{Wst} = \left(N_W - N_{CVaR}^s\right) p_{wst} \\ p_{Wst}^{TH} = \left(N_W - N_{CVaR}^s\right) p_{wst}^{TH} \\ k_1^T, k_1^N \in [1, +\infty), k_2^T, k_2^N \in (0, 1] \end{array} \right\} \tag{26}$$

$$\widehat{\Omega}_{GF} = \left\{ p_s(Z_s) \;\middle|\; \begin{array}{l} p_k(Z_s) \geqslant p_s(Z_s) - \widehat{p}_0(Z_s), s \in S_T \\ p_k(Z_s) \geqslant \widehat{p}_0(Z_s) - p_s(Z_s) s \in S_T \\ \partial_1 \widehat{p}_0(Z_s) \leqslant p_s(Z_s) \leqslant \partial_2 \widehat{p}_0(Z_s), s \in S_T \\ \sum_{s\in S_T} p_s(Z_s) = \dfrac{T_D}{365} \\ \sum_{s\in S_T} p_k(Z_s) \leqslant \psi \\ \sum_{s\in S} p_s(Z_s) = 1 \\ p_s(Z_s), p_k(Z_s) \geqslant 0 s \in S \\ S = S_T \cup S_N \end{array} \right\} \tag{27}$$

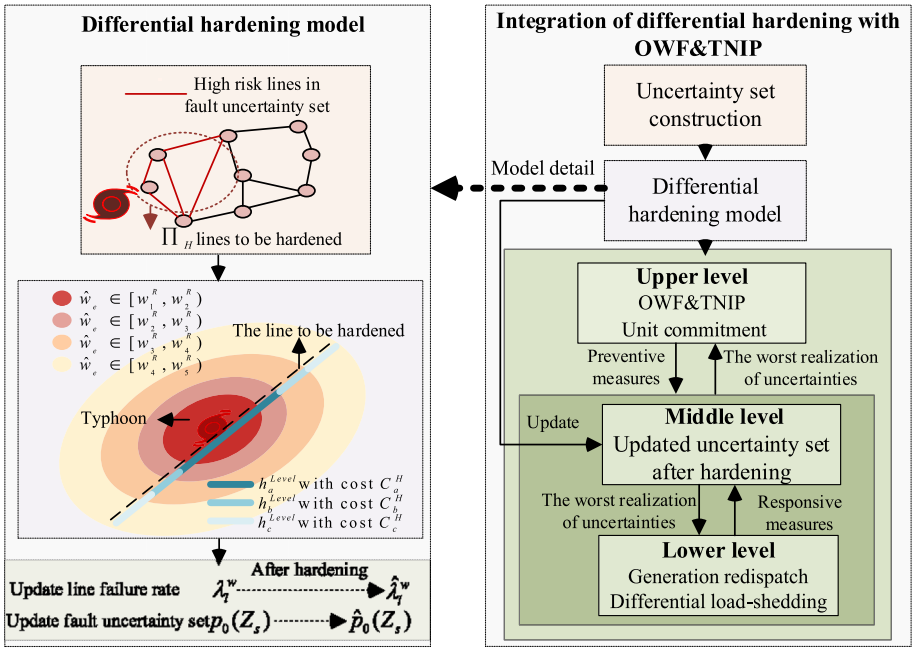

Fig. 6. The differential hardening model and the process of its integration with ROWF&TNIP.

3.5. Lower level constraints

(1) Generation redispatch constraints

$$u^o_{gst}P^{\min}_g \le p_{gst} \le u^o_{gst}P^{\max}_g, \forall g \in G, \forall s \in S, \forall t \in T \tag{28}$$

where $P^{\min}_g, P^{\max}_g$ are minimum and maximum output of generator g.

(2) Power flow constraints

$$p_{lst} - B_l\left(\theta_{s(l)t} - \theta_{e(l)t}\right) \ge -M(1-x_l), \quad \forall s \in S, \forall t \in T, \forall l \in L_c \tag{29}$$

$$p_{lst} - B_l\left(\theta_{s(l)t} - \theta_{e(l)t}\right) \le M(1-x_l), \quad \forall s \in S, \forall t \in T, \forall l \in L_c \tag{30}$$

$$-x_l\underline{p}_l \le p_{lst} \le x_l\overline{p}_l, \quad \forall s \in S, \forall t \in T, \forall l \in L_c \tag{31}$$

$$p_{lst} = z^*_l B_l\left(\theta_{s(l)t} - \theta_{e(l)t}\right), \forall s \in S, \forall t \in T, \forall l \in L_e \tag{32}$$

$$-\overline{p}_l \le p_{lst} \le \overline{p}_l, \quad \forall s \in S, \forall t \in T, \forall l \in L_e \tag{33}$$

where $B_l, \overline{p}_l$ are admittance and maximum transmission capacity of line l, $\theta_{s(l)t}, \theta_{e(l)t}$ are phase angles of the starting and ending nodes of line l, M is a sufficient large positive number, z^*_l is fault state of line l determined during the construction of fault uncertainty set.

(3) Differential load-shedding and other constraints

$$0 \le p_{r_1st} \le k_{r_1}p_{bst}, \quad \forall t \in T, \forall r_1, b \in B \tag{34}$$

$$0 \le p_{r_2st} \le k_{r_2}p_{bst}, \quad \forall t \in T, \forall r_2, b \in B \tag{35}$$

$$k_{r_1} + k_{r_2} = 1 \quad \forall r_1, r_2 \in B \tag{36}$$

$$0 \le p_{r_wst} \le p_{Wst}, \quad \forall t \in T, \forall W \in L_W \tag{37}$$

$$\sum_{g\in G} p_{gst} + \sum_{W, r_w \in L_W}\left(p_{Wst} - p_{r_wst}\right) + \sum_{l\in L^+(b)} p_{lst} - \sum_{l\in L^-(b)} p_{lst} = \sum_{p_{r_1t}, p_{r_2}, b\in B}\left(p_{bst} - p_{r_1st} - p_{r_2st}\right) \tag{38}$$

where p_{bst} is load at bus b at time t under scenario s, k_{r_1}, k_{r_2} are percentage of important and normal load. $L^+(b), L^-(b)$ are sets of lines of which power flow in and out from bus b. The feasible region $\mathscr{H}$ of lower-level problem is (28)–(38).

4. Problem solution

The proposed ROWF&TNIP model is a tri-level optimization problem, with binary variables in the upper level and continuous variables in the middle and lower level. In light of C&CG method [22], we develop a decomposition algorithm with a master-subproblem framework to solve this problem. At the first iteration of this algorithm, the differential hardening is firstly implemented to update the theoretical fault probability distribution before the start of planning process. Then, acquiring the worst-case OWF outputs and actual grid faults probability distribution searched by the subproblem, the master problem finds the optimal planning and operational measures and lower bound (LB). The subproblem leverages the master's outputs to determine the worst-case realization of uncertain factors in uncertainty set and computes the upper bound (UB). It then constructs corresponding C&CG cuts, feeding them back to the master problem for the next iteration. This process continues until the gap between the LB and UB is small enough for the algorithm to converge. For brevity, we denote the ROWF&TNIP model in compact matrix form, and the illustration of the compact variables and constraints are shown in Table 1.

The objective function (15)–(17) is denoted as (39)–(41).

Table 1
Illustration of compact variables and constraints.

Compact form		Meaning
Variables	$\mathbf{x}$	Variables in upper level $x_l, x_w, u^o_{gs}t, u^S_{gs}t, u^D_{gs}t$
	$\mathbf{P(z)}, \mathbf{P_w}$	Variables in middle level $p_s(Z_s), p_{wst}$
	$\mathbf{y}$	Variables in lower level $p_{gst}, p_{r_wst}, p_{r_1st}, p_{r_2st}$
	$\boldsymbol{\beta}$	Dual variables corresponding to constraint (45)
	$\mathbf{c}_1, \mathbf{c}_2$	Cost of $\mathbf{x}, \mathbf{y}$, respectively
	$\overline{\mathbf{w}}, \underline{\mathbf{w}}$	Binary variables corresponding to $\Delta\overline{\mathbf{P}}_\mathbf{w}, \Delta\underline{\mathbf{P}}_\mathbf{w}$, $\overline{w}_i, \underline{w}_j$ are their elements
Parameters	$\mathbf{A}, \mathbf{B}, \mathbf{C}, \mathbf{D}, \mathbf{F}, \mathbf{a}, \mathbf{b}, \mathbf{c}, \mathbf{d}$	Constant matrices/vectors of constraints in compact form
	$\mathbf{z}$	Constant vector of line fault state z^*_l
	$\mathbf{E(x, z)}$	Constant matrix related to $\mathbf{x}, \mathbf{z}$ in lower level constraints (28)–(32)
	$\Delta\overline{\mathbf{P}}_\mathbf{w}, \Delta\underline{\mathbf{P}}_\mathbf{w}$	Constant vectors of upper and lower deviation degree of $\mathbf{P_w}$
	$\mathbf{P^0_w}$	Constant vectors of theoretical value of $\mathbf{P_w}$
	Γ^W	Budget of the binary deviation variables $\overline{w}_i, \underline{w}_j$

$$\min_{\mathbf{x}\in\mathscr{X}}\left\{\mathbf{c}_1{}^{\mathrm{T}}\mathbf{x} + \max_{\substack{\mathbf{P(z)}\in\Omega_{GF}\\ \mathbf{P_w}\in\Omega_{WFO}}} E[f(\mathbf{x}, \mathbf{P(z)}, \mathbf{P_w})]\right\} \tag{39}$$

$$\max_{\substack{P(Z)\in\Omega_{GF}\\ P_w\in\Omega_{WFO}}} E[f(x, P(z), P_w)] = \max_{\substack{P(Z)\in\Omega_{GF}\\ P_w\in\Omega_{WFO}}}\left[\sum_{s\in S} f(x, P(z), P_w)p_s(Z_s)\right] \tag{40}$$

$$f(\mathbf{x}, \mathbf{P(z)}, \mathbf{P_w}) = \min_{\mathbf{y}\in\mathscr{H}} \mathbf{c}_2{}^{\mathrm{T}}\mathbf{y} \tag{41}$$

The upper level feasible zone $\mathscr{X}$ includes constraints (19)–(20), which can be denoted as (42).

$$\mathbf{Ax} \le \mathbf{a} \tag{42}$$

The middle level feasible zone includes Ω_{WFO}, $\widehat{\Omega}_{GF}$, which can be denoted as (43)–(44), respectively.

$$\mathbf{BP(z)} \le \mathbf{b} \tag{43}$$

$$\mathbf{CP_w} \le \mathbf{c} \tag{44}$$

The lower level feasible zone $\mathscr{H}$ includes constraints (28)–(38), which can be denoted as (45)

$$\mathbf{Dy} + \mathbf{E(x, z)y} + \mathbf{FP_w} \ge \mathbf{d} \tag{45}$$

In (45), $\mathbf{x}, \mathbf{z}, \mathbf{P_w}$ are determined by upper and middle level problem, so that the lower level is a linear programming problem with continuous decision variable $\mathbf{y}$. Therefore, duality transformation is performed and to convert lower level problem to max problem and merge it with the middle level problem as (46)–(48).

$$\max_{\boldsymbol{\beta}, \mathbf{P(z)}, \mathbf{P_w}}\left\{\left[(\mathbf{d} - \mathbf{FP_w})\right)^{\mathrm{T}}\boldsymbol{\beta}\right]\right\} \tag{46}$$

$$\left[\mathbf{D} + \mathbf{E(x, z)y}\right]^{\mathrm{T}}\boldsymbol{\beta} \le p_s(Z_s)\mathbf{c}_2, \forall s \in S \tag{47}$$

$$(41) - (42), \boldsymbol{\beta} \ge 0 \tag{48}$$

Given that $\mathbf{P_w}{}^{\mathrm{T}}\boldsymbol{\beta}$ is a bilinear item and the maximum value of (46) is attained at the upper or lower bound of the budget uncertainty set of $\mathbf{P_w}$, (46) can be rewritten as (49)–(50) and the big-M method can be employed to linearize it [6].

$$\max_{\boldsymbol{\beta}, \mathbf{P(z)}, \mathbf{P_w}}\left\{\left[\left(\mathbf{d} - \mathbf{F}\left(\mathbf{P^0_w} + \overline{\mathbf{w}}\Delta\overline{\mathbf{P}}_\mathbf{w} - \underline{\mathbf{w}}\,\Delta\underline{\mathbf{P}}_\mathbf{w}\right)\right)\right)^{\mathrm{T}}\boldsymbol{\beta}\right]\right\} \tag{49}$$

$$\begin{cases} P_w = P_w^0 + \overline{w}\Delta\overline{P}_w - \underline{w}\Delta\underline{P}_w \\ \sum_{i\in N_{\overline{w}}, j\in N_{\underline{w}}} \left(\overline{w}_i + \underline{w}_j\right) \leqslant \Gamma^W \\ \overline{w} + \underline{w} = 1, \overline{w}, \underline{w} \text{arebinaryvectors} \end{cases} \tag{50}$$

The original tri-level min-max-min problem is now transformed into a bi-level min-max problem as (51).

$$\min_{x\in\mathcal{G}} \left\{ c_1^{\mathrm{T}} x + \max_{\beta, P(z), P_w} \left\{ \left[\left(d - F\left(P_w^0 + \overline{w}\Delta\overline{P}_w - \underline{w}\Delta\underline{P}_w\right)\right)^{\mathrm{T}} \beta \right] \right\} \right\} \tag{51}$$
$$\text{s.t}(40)-(42),(45)-(46),(48)$$

The detailed process of the primal-dual decomposition algorithm is as follows.

Step 1: Initialization. Initialize LB, UB, max iteration M_e, converge gap ν, $m = 1$, C&CG cuts $\phi^a = \varnothing$.

Step 2: If $m = 1$, the differential hardening is firstly implemented to update the theoretical fault probability distribution before the start of planning process. Then, for $m = 1, \ldots, M_e$, solve master problem (52)–(54), record the solution $\mathbf{x}^{(m)}$, $\alpha^{(m)}$, optimal value $V_{MP}^{(m)}$, updates $LB = V_{MP}^{(m)}$.

$$\min_{\alpha, \mathbf{x}\in\mathcal{G}} \mathbf{c}_1{}^{\mathrm{T}}\mathbf{x} + \alpha \tag{52}$$

$$\mathbf{Ax} \leq \mathbf{a} \tag{53}$$

$$\text{C\&CG cuts}: \phi^a \tag{54}$$

Step 3: Solve sub-problem (55)–(56), record the solution $\mathbf{P}(\mathbf{z})^{(m)}$, $\boldsymbol{\beta}^{(m)}$, $\mathbf{P_w}^{(m)}$ and the optimal value $V_{SP}^{(m)}$, then update $UB = LB + V_{SP}^{(m)} - \alpha^{(m)}$.

$$\max_{\boldsymbol{\beta}, \mathbf{P}(\mathbf{z}), \mathbf{P_w}} \left\{ \left[\left(\mathbf{d} - \mathbf{F}\left(\mathbf{P_w^0} + \overline{\mathbf{w}}\Delta\overline{\mathbf{P}}_\mathbf{w} - \underline{\mathbf{w}}\,\Delta\underline{\mathbf{P}}_\mathbf{w} \right) \right) \right)^{\mathrm{T}} \boldsymbol{\beta} \right] \right\} \tag{55}$$

$$\begin{cases} \left[\boldsymbol{D} + \boldsymbol{E}\left(\boldsymbol{x}^{(m)}, \boldsymbol{Z}\right)\boldsymbol{y} \right]^{\mathrm{T}} \boldsymbol{\beta} \leqslant p_s(Z_s) c_2, \forall s \in S \\ (46), (48) \end{cases} \tag{56}$$

Step 4: If $UB - LB \leq \nu$, the algorithm is converged, otherwise, go to next step.

Step 5: Primal and dual cuts generation. Generate C&CG primal cuts (57) based on the subproblem objective function and its feasible zone, and add them to $\boldsymbol{\beta}^{(m)}$, $m = m + 1$, turn to step 2.

$$\begin{cases} \alpha \geqslant \sum_{s\in S} \left(c_2^{\mathrm{T}} \boldsymbol{y}^{(m+1)} p_s^{(m)}(Z_s) \right) \\ \left[\boldsymbol{D} + \boldsymbol{E}\left(\boldsymbol{x}^{(m)}, \boldsymbol{z}\right)\boldsymbol{y}^{(m+1)} + \boldsymbol{F}\boldsymbol{P}_w^{(m)} \geqslant \boldsymbol{d} \right. \end{cases} \tag{57}$$

Both the master problem and subproblem are mixed integer linear programming (MILP) which can be solved by the commercial solver. The whole process of the proposed algorithm is shown in Fig. 7.

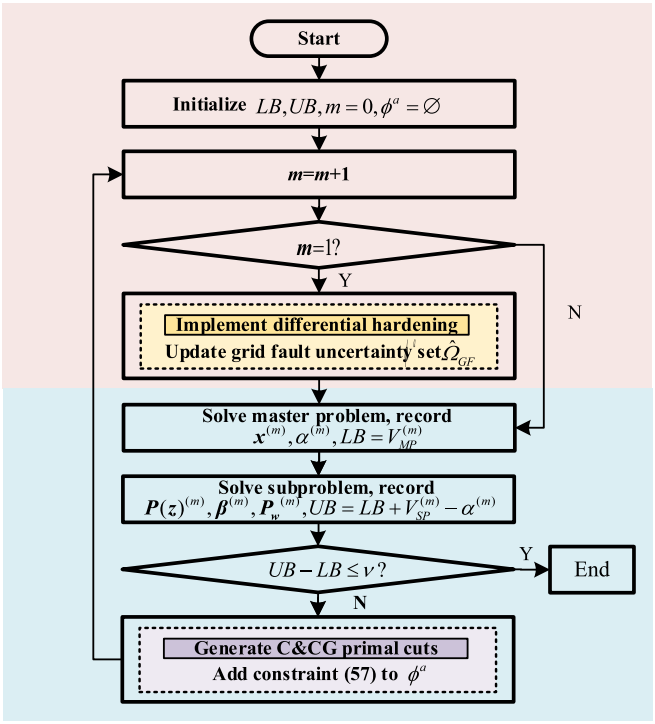

Fig. 7. The process of the primal-dual decomposition algorithm.

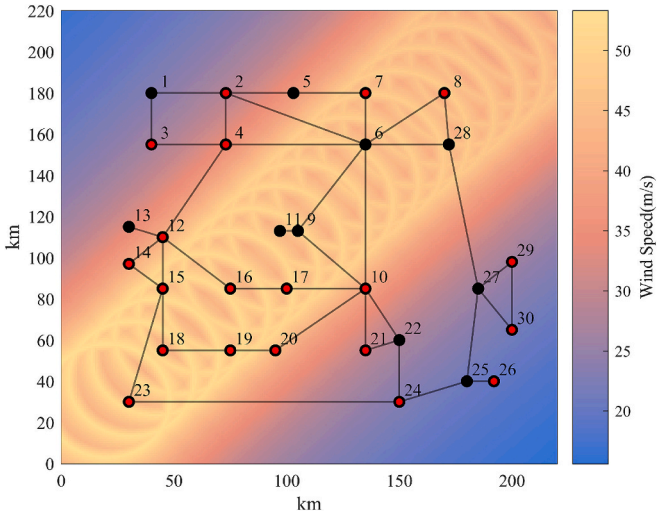

Fig. 8. The 30-bus system topology and the typhoon dynamics.

5. Case study

5.1. Modified IEEE-30 bus test system and model coefficients illustration

The modified 30-bus system assumed to be located in an area of 48,400 km^2 consists of 41 existing and 8 traditional power plant totaling 24,000 MW generation capacity, 3600 MW OWF to be integrated, and 21,000 MW peak load. We assume all generators in a power plant keeps the same operation mode, and in the following text, "generator" refers to power plant connected at each bus. The detailed parameter setting of the generators are presented in Appendix Table B1, and the load curve is presented in Appendix Fig.B.1. Buses 3, 12, 13, 14, 15, 18, and 23 are available for OWF integration, with each bus integrating 1200 MW OWF. The simulated typhoon makes landfall at bus 23 with 15 km/h moving speed and 52 m/s initial max wind speed. The 30-bus system topology and the typhoon dynamics are presented in Fig. 8, where the load node is marked with red color. In OWF output uncertainty set, k_E under TDS when typhoon speed are above 12 m/s is set to 20 % and k_E under NOS is set to 15 %, respectively. The Γ^W is set to 50. The theoretical turbine output curves of OWF at all 7 buses under NOS are assumed to be same and shown in Fig. 1(a), while under TDS, OWF at different buses present different theoretical turbine output curves, four typical turbine output curves and their variation zone at buses 3, 13, 14, 23 under TDS are presented in Appendix Fig. B2. The load curve is presented in Fig. B2. For failed turbines CVaR model, we assume individual turbine capacity is 10 MW, so that N_W is 120 for each OWF and the confidential level β is 99 %. In grid fault uncertainty set, we consider average 20 typhoon days of a year, T_D=20. Given that line failure rate uncertainty is also mainly resulted by wind speed forecasting error, ∂_1, ∂_2 take the value of 0.8 and 1.2, consistent with k_E under TDS. In differential hardening model strategy 1, wind speed interval is segmented

starting from 27 m/s to 53 m/s, with a step difference of 4 m/s, such as $w_1^R \sim w_2^R$ is 27 m/s ~ 31 m/s, the $h_a^{Level} \sim h_c^{Level}$ and $C_a^H \sim C_b^H$ corresponding to each wind speed interval are shown in Appendix Table B2, and the $h_a^{Level} \sim h_c^{Level}$ and $C_a^H \sim C_b^H$ corresponding to hardening strategy 3 are shown in Appendix Table B3. The other main coefficients of uncertainty sets and ROWF&TNIP model are shown in Table 2. The program is developed with Matlab R2022a on a PC with Intel(R) core (TM) i5-7200U.

5.2. Comparative analysis of effectiveness of the proposed ROWF&TNIP model

To validate the effectiveness of the proposed multi-scenario distributionally robust ROWF&TNIP model on enhancing resilience with less conservatism, we design four cases based on different benchmark models to compare with ours.

Case 1. (C1) ~ Case 2 (C2) are based on single scenario distributionally robust model, targeting for validation of the effectiveness of the multi-scenario setting. To be specific, C1 only considers NOS, that is, the average annual typhoon days T_D= 0 and the days of NOS T_N=365, while C2 only considers TDS, that is, T_D=20 and T_N=0.

Case 3. (C3) is based on multi-scenario robust model, aiming to validate the effectiveness of the distributionally robust setting. This benchmark model is the widely used robust model which searching the high-loss faults based on the N—K uncertainty set, such as [18,24]. It also follows the tri-level min-max-min framework, and the main differences it and the proposed model lies in a) it ignores the probability distribution of all possible fault scenarios under TDS, and b) it only focuses on the high-loss fault, ignoring the other possible fault types under TDS. The detailed form of this model is presented in Appendix C.

Case 4. (C4) is based on the proposed model without the CVaR setting. In this case, our CVaR-based budget uncertainty set for OWF output reduces to a widely used budget uncertainty set which ignores the turbine failure risk, such as [5]– [6]. The detailed form of this model is also presented in Appendix C.

Case 5. (C5) is based on the proposed multi-scenario distributionally robust model, which serves as the reference case for all subsequent case studies.

First, we search for nine N-4 fault scenarios, with three scenarios each for high probability, high loss, and cascading fault and report them in Table 3, and the fault lines are represented in the form of line number, and the corresponding relationship between the line number and the starting-end nodes is presented in Appendix Table C1. Moreover, the normalized theoretical probability distribution of these fault scenarios and the worst-case probability distribution searched by the middle-level problem are shown in Fig. 9. In contrast to the theoretical probability distribution, in the worst-case probability distribution scenario, the probabilities of all high-loss faults have increased by 18 % ~ 20 %, and the probabilities of the first and the second high-probability and cascading faults have also risen by 20. Meanwhile, the probabilities of the third high-probability and cascading faults have decreased by 15 %

Table 2
Results of RTEP with different contingency severity.

Coefficients	Value	Coefficients	Value
Uncertainty set		C_w^{WF}	0.6 M¥/(MW·year)
w_{ci}, w_{co}, w_R	3 m/s,12 m/s,25 m/s	$p_g^{\min}$	$0.3p_g^{\max}$
$\lambda_w^{norm}, \lambda_l^{norm}$	0.03,0.02	$\prod_H$	15
p_l^R	$0.7p_l^{\max}$	k_{r_1}, k_{r_2}	0.2, 0.8
ROWF&TNIP model		$C_{r_1}^{LS}, C_{r_2}^{LS}$	10¥/kWh, 1¥/kWh
C_l^L	0.7 M¥/(km·year)	$C_{r_w}^{WC}$	0.4¥/kWh

Table 3
Results of 9 Fault Scenarios.

No.	High-probability fault	No.	High-loss fault	No.	Cascading fault
1	20,30,32,41	4	7,9,15,23	7	8,9,10,40
2	22,23,24,26	5	6,10,11,41	8	21,23,25,26
3	7,8,23,24	6	15,21,22,27	9	22,19,10,8

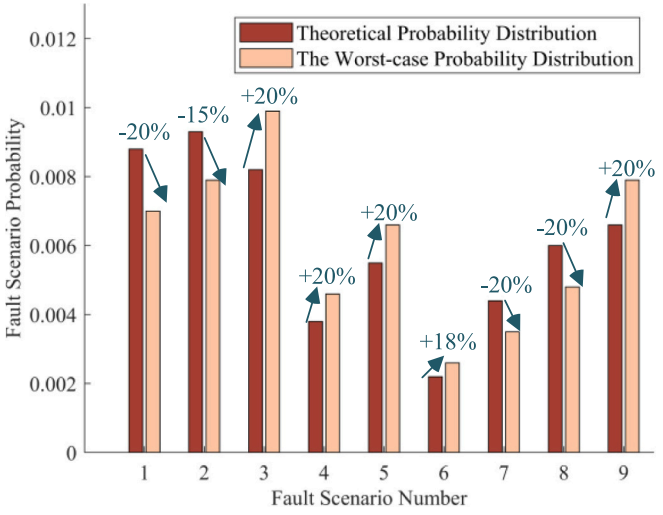

Fig. 9. The probability distribution results of nine fault scenarios.

~ 20 %, indicating that in the worst-case fault probability distribution, the probability of the fault scenarios with higher losses tends to increase.

Then, we analyze the ROWF&TNIP results of 30-bus system in Table 4. It worths mentioning that since the OWF investment cost remains 2.16B¥, the investment cost in all tables only encompasses line investment to reflect the variation of results. Moreover, in all cases, there is no load-shedding under NOS, and we also present the OWF integration bus and line expansion plan. Specially, for C1 ~ C3, it takes two steps to obtain the planning and operation costs. Firstly, the investment cost and planning scheme are obtained by model used in C1 ~ C3, then operational simulations are conducted under 20 typhoon days and the grid uncertainty set used in C5 to calculate generation, wind-curtailment and load-shedding cost. Taking the sum of investment, hardening, generation and wind-curtailment cost as economic index, the load-shedding cost as resilience index, the following conclusions can be drawn.

i) The effectiveness of multi-scenario setting. Upon comparison of single scenario model which focus exclusively on either NOS or TDS, the proposed multi-scenario model exhibits the lower total cost, signifying that consideration for both NOS and TDS achieves a more balanced coordination of resilience and economic efficiency. Taking C1, C2 and C5 for example, in C5, the economic index is 47.629B¥, and the resilience index load-shedding cost is 0.039B¥. Compared with C1, the economic index increases by 0.217B¥, while the resilience index decreases by 1.349B¥, suggesting that the planning scheme focus solely on NOS would suffer losses exceeding the reduced grid construction costs in the event of a severe typhoon disaster, while compared with C2, the economic index decreases by 0.019B¥, and the resilience index decreases by 0.015B¥, indicating that the planning scheme only considers TDS is less cost-efficient and overly conservative. To better observe the system's resilience performance of C1, C2 and C5, we present hourly load-shedding under TDS by the means of expected load percentage defined by (58) in Fig. 10. It can be seen that the load-shedding in C2 and C5 is significantly lower than that in C1, verifying the effectiveness of the planning scheme in resilience enhancement.

ii) The effectiveness of distributionally robust setting. Upon

Table 4
Results of ROWF&TNIP based on Different Model with IEEE 30-bus System.

IEEE 30-bus system ROWF&TNIP results (B¥)	Single scenario distributionally robust model (No TDS)	Single scenario distributionally robust model (No NOS)	Multi-scenario robust model	Multi-scenario distributionally robust model (No CVaR)	The proposed multi-scenario distributionally robust model
Total Cost	48.800	47.702	47.730	47.668	47.684
Investment Cost	0.117	0.239	0.279	0.239	0.218
Hardening Cost	0.045	0.045	0.045	0.045	0.045
Generation Cost	47.249	47.363	47.372	47.362	47.380
Wind-curtailment Cost	0.002	0.002	0.002	0.004	0.002
Load-shedding Cost	1.388	0.054	0.032	0.018	0.039
OWF integration bus	3,18,23	3,18,23	3,13,23	3,18,23	3,12,23
Line expansion plan	16,24,28,31,35,38	9,10,16,21,23,24, 25,28,31,35,38	9,10,16,21,23,24, 25,28,30,31,35,38	9,10,16,21,23,24, 25,28,31,35,38	9,10,16,21,24, 25,28,31,35,38

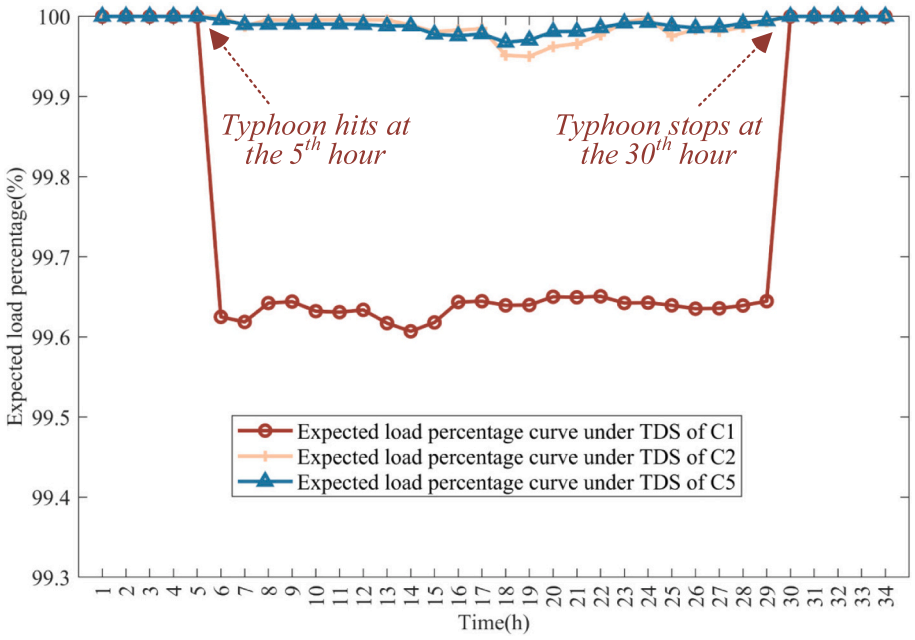

Fig. 10. Expected load percentage curve under TDS of C1, C2, C5.

comparison of results of the multi-scenario robust model, the proposed model provides a more cost-effective planning scheme. For 30-bus system, the robust model obtains 0.032B¥ resilience index and 47.698B¥ economic index, compare with the proposed model, the decrease in economic index is 0.069B¥, significantly greater than the increase in resilience index 0.007B¥. The robust model tends to invest more lines for resisting high-loss faults, however, the more expansive planning scheme may not effectively prevent the high-probability or cascading faults.

iii) The effectiveness of the CVaR setting. Upon comparison of the model without CVaR, the proposed model obtains a more costly planning scheme, indicating that the ignore of turbine failure risk tend to underestimate the impact of typhoon disasters and overestimate the OWF output during TDS. To be specific, compared with C5, the investment and wind-curtailment cost of C4 increase by 0.021B¥ and 0.002B¥ to improve absorption of OWF output, while the generation and the load-shedding cost decrease by 0.018B¥, 0.021B¥ due to more OWF output participating in load supply, resulting the 0.016B¥ decrease in total cost. Although the CVaR setting leads to a slightly more costly planning scheme, its main contribution is to objectively capture the turbine failure risk under TDS and ensure the planning model more in line with reality, rather than reduce the conservatism of model.

$$LP(t) = \sum_{s\in S_T}\left[\widehat{p}_s(Z_s)\frac{\sum_{r,b\in B}(p_{bst}-p_{rst})}{\sum_{b\in B}p_{bst}}\right], \forall t \in T \tag{58}$$

5.3. Sensitivity analysis of uncertainty set parameters

In this part, we design a series of case studies to investigate the planning results under varying uncertain factors scenarios, and assess the resilience and economy performance.

5.3.1. Sensitivity analysis of OWF output uncertainty set parameters

To study the optimal planning schemes under different scenarios of turbine failures and turbine outputs in the OWF output uncertainty set, two groups of cases with different CVaR confidence level and wind speed forecasting error are designed. Case group 1 consists of three cases C5 and Case 6 (C6) ~ Case 7 (C7), each corresponding to the CVaR confidence level β=80 %(C6), 90 %(C7), 99 %(C5). Case group 2 consists of three cases C5, Case 8 (C8) ~ Case 9 (C9), each corresponding to the forecasting error under TDS k_E=10 %(C8), 20 %(C5), 30 %(C9), and the k_E under NOS is 5 percentage points lower than TDS.

Firstly, we select four candidate OWF integration buses (buses 13,14,15,23) as examples to report the probability density functions

(PDF) of failed turbines and CVaR of failed turbines N_{CVaR} in Fig. 11. With the β increases from 80 % to 99 %, the N_{CVaR} of OWF at buses 13 and 23 increases from 39 to 48, 17 to 24, respectively. The OWF at bus 14,15 are close to the typhoon landing area, leading to higher turbine failure rate and the same turbine failures' PDF. With the β increases from 80 % to 99 %, the N_{CVaR} of OWF at these buses 14,15 increase from 46 to 55.

The detailed indices of C5 ~ C9 are listed in.

Table 5 With β escalating from 80 % to 99 %, the number of failed turbines under TDS increases, leading to an decrease in OWF power generation and an increase of the generation cost under TDS. However, the investment, generation and load-shedding cost fail to show a monotonic change with the increase in the number of turbine failures. On one hand, the increase in thermal units power generation can replace the output of the failed turbines, on the other hand, taking C7 for example, more lines might be invested to offset the decrease in OWF output. As k_E rises from 10 % to 30 %, both the generation cost under TDS and NOS increase, and the total generation cost increases from 47.263B¥ to 47.995B¥. Since the wind-curtailment in the system is minimal, the worst-case OWF output scenario tends to result in less OWF output and more power generation from thermal units, so as to increase the total generation cost. Therefore, the greater the wind speed forecasting error is, the lower the bound of OWF output will be, resulting the increase in both TDS and NOS generation cost. However, as k_E rises from 10 % to 30 %, the planning scheme remains unchanged, and the load-shedding does not change monotonically either. This indicates that the change in the OWF output is not sufficient to alter the planning scheme, and under the combined influence of OWF output decreases and thermal units output increases, the load shedding will not exhibit a specific variation trend.

5.3.2. Sensitivity analysis of grid fault uncertainty set parameters

To study the optimal planning schemes under different grid fault severity and theoretical and actual probability distribution deviation degree, two groups of cases with different *N*—*K* level and deviation degree coefficients ∂_1, ∂_2 are designed. Case group 1 consists of three cases C5 and Case 10 (C10) ~ Case 11 (C11). In C10 and C11, the fault uncertainty set consists of nine *N*-2 and *N*-3 fault scenarios, respectively. C5 corresponds to *N*-4 level. Case group 2 also consists of three cases C5, Case 12 (C12) ~ Case 13 (C13), each corresponding to the $\partial_1 = 1, \partial_2 = 1$ (C12), $\partial_1 = 0.8, \partial_2 = 1.2$ (C5), $\partial_1 = 0.6, \partial_2 = 1.4$%(C13). The planning and operational cost results are reported in Fig. 12.

From C10, C11 to C5, the fault severity degree rises, and the total cost increases from 47.648B¥ to 47.684B¥. However, the line investment, generation cost and load-shedding cost do not increase monotonically as the *N*—*K* level increases. For example, the load-shedding cost and generation cost of C11 (N-3 level) are 0.03B¥ and 47.361B¥, respectively, which are the smallest of the three cases, while the line investment is 0.221B¥, which is the largest. These results reveal that increases from 51.998B¥ to 52.295B¥, wind power cost increases from 47.648B¥ to 47.684B¥, and the economic index improves from 55.060B¥ to 55.917B¥. The load-shedding escalates from 0.031B¥ in C10 to 0.053B¥ in C5, and then declines to 0.048B¥ in C12. These results reveals that a more severe *N*—*K* level does not necessarily require more line investment or load shedding. However, it does necessitate the implementation of more costly planning and operational measures for resilience. Since the worst-case fault probability distribution tends to increase the probability of faults with higher losses, as the theoretical and actual probability distribution deviation degree increases from C12 to C13, the total cost increases from 47.679B¥ to 47.699B¥. The line investment increases from 0.218B¥ to 0.239B¥, while the generation cost and load-shedding cost do not increase monotonically, which also indicates that a more conservative fault uncertainty set can result in a more costly planning and operation scheme.

5.4. Sensitivity analysis of short-term measure parameters

The proposed ROWF&TNIP model incorporates three typical short-term source-network-load measures: preventive unit commitment, differential hardening and differential load-shedding To reveal how these measures influence the resilience and economy of the planning results, we design the following case studies.

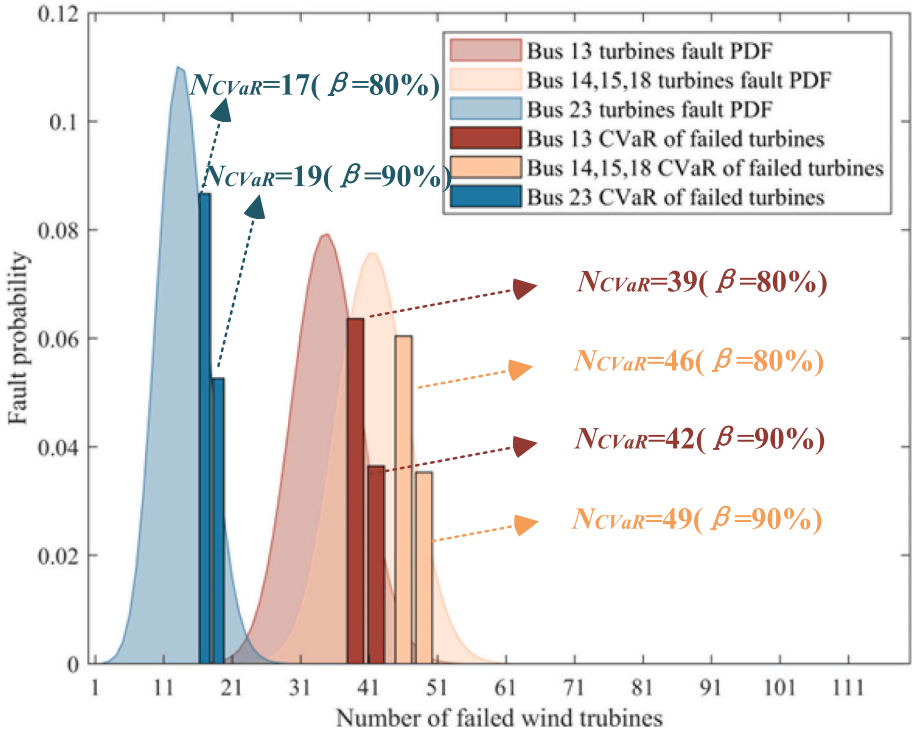

Fig. 11. PDF and N_{CVaR} of OWF at buses 13,14,15,18,23.

Table 5
Results of Rowf&tnip with Different OWF Output Uncertainty.

Cost(B¥)	Total Cost	Investment Cost	Generation Cost	TDS Generation Cost	NOS Generation Cost	Wind-curtailment Cost	Load-shedding Cost
β=80 %	47.683	0.218	47.393	1.208	46.185	0.004	0.023
β=90 %	47.682	0.239	47.378	1.213	46.165	0.002	0.018
β=99 %	47.684	0.218	47.380	1.215	46.165	0.002	0.039
k_E=10 %	47.553	0.218	47.263	1.205	46.058	0.004	0.023
k_E=20 %	47.684	0.218	47.380	1.215	46.165	0.002	0.039
k_E=30 %	48.288	0.218	47.995	1.237	46.300	0.003	0.027

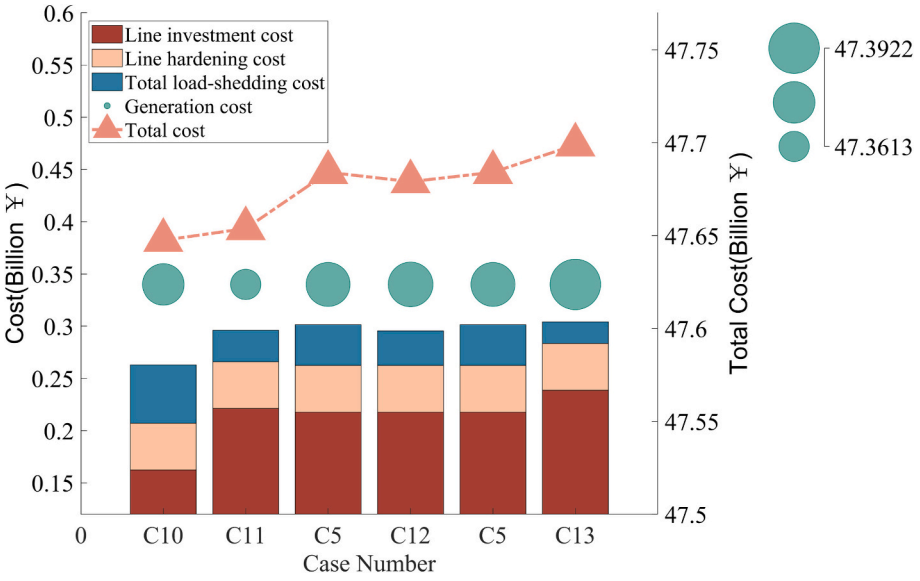

Fig. 12. Cost results with different fault uncertainty set parameters.

5.4.1. Sensitivity analysis of differential hardening strategy settings

In this part, we design 20 cases, applying three hardening strategies to 0, 5, 10, 15, and 20 lines in the fault uncertainty set, to analyze the cost-benefit of differential hardening strategies. First, we consider the 20 different lines included in the N-4 fault uncertainty set as the lines to be hardened, dividing the lines into 1 km segments and categorizing the wind speed intervals by 4 m/s increments, with hardening levels set according to a 2 m/s wind speed difference (the wind speed intervals and corresponding hardening levels and hardening costs are shown in Appendix B). We then count the cumulative number of line segments at each hardening level for each line, as shown in Fig. 13. Subsequently, we design three differential hardening strategies. Strategy 1 involves segment strategy as described in Appendix Table B2, which is also the strategy adopted by the benchmark case C5. Strategy 2 does not harden the lines by segment but rather hardens the entire line based on the maximum wind speed it experiences based on the hardening level and wind speed correspondence in Appendix Table B1. Strategy 3 adopts a more easy segment hardening plan, where line segments with a maximum wind speed of 43 m/s or less are hardened according to a design wind speed of 33 m/s, and all other line segments are hardened according to a design wind speed of 37 m/s, as shown in Appendix Table B2. All three strategies prioritize hardening of lines with high failure rates. The detailed costs associated with each case are depicted in Fig. 14, and the economic index and resilience index are summarized in Table 6. It worth mentioning that the economic cost here also includes the OWF output cost calculated based on average Chinese OWF generation cost 0.4¥/kWh. The following four conclusions from different perspectives can be drawn.

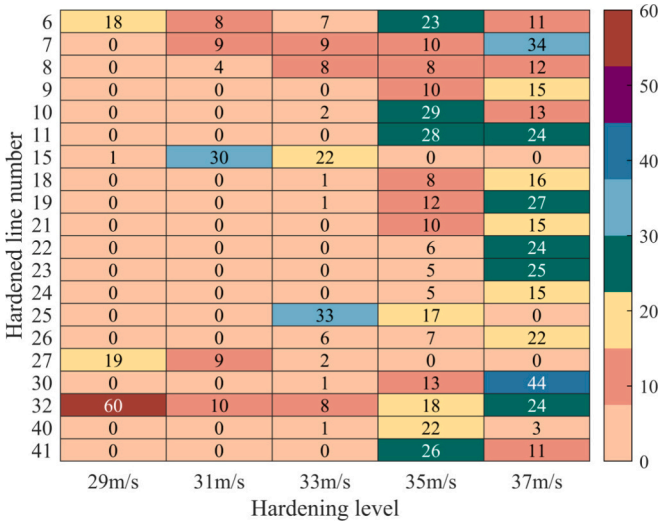

Fig. 13. The number of line sectors under each hardening level.

i). Economically, economic cost for hardening 5 lines with strategy 1 is 49.140B¥, the lowest among the 20 cases. For hardening 5, 15, 20 lines, strategy 1 is the most economical. This indicates the effectiveness of detailed differential hardening strategy in reducing total cost and relieving model conservatism.

ii). In terms of resilience, hardening 15 lines with strategy 1 results in the least load-shedding cost 0.019B¥, and when hardening 5, 10, 15 lines, the strategy 1 achieve the lower load-shedding than strategy 2 and strategy 2, verifying the effectiveness of detailed differential hardening strategy in resilience enhancement.

iii). Regarding the total cost, hardening 20 lines with strategy 2 incurs the highest total cost 49.194B¥, which is even 0.005B¥ more than

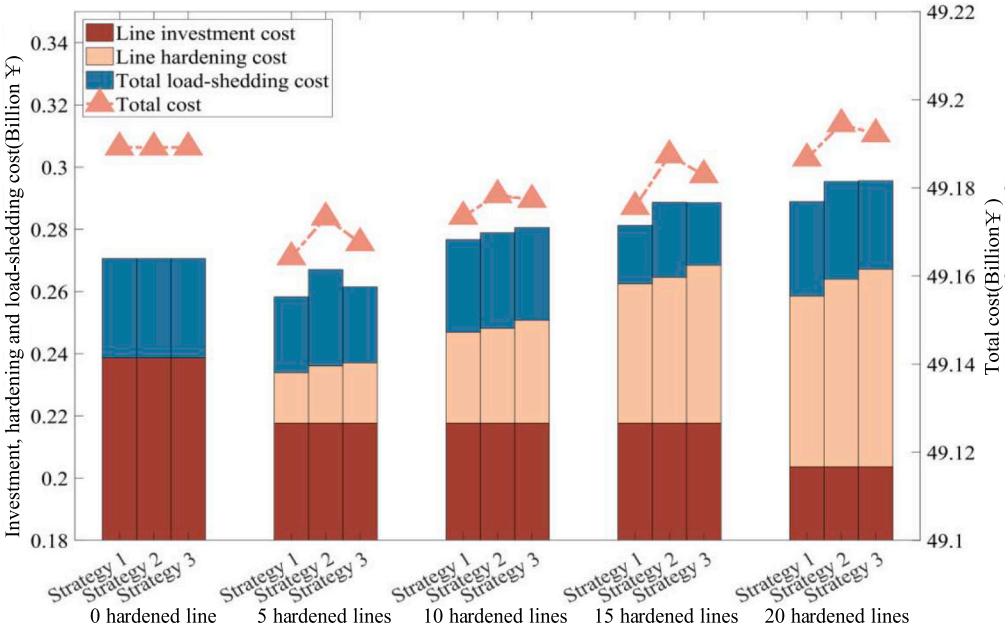

Fig. 14. Costs with different hardening strategies and hardening budgets.

Table 6
Results of ROWF&TNIP with Different Hardening Strategy.

Hardened lines	TC(B¥)			Economic index(B¥)			Resilience index(B¥)		
	Strategy 1	Strategy 2	Strategy 3	Strategy 1	Strategy 2	Strategy 3	Strategy 1	Strategy 2	Strategy 3
0	49.189	49.189	49.189	49.157	49.157	49.157	0.032	0.032	0.032
5	49.164	49.173	49.167	49.140	49.142	49.143	0.024	0.031	0.024
10	49.173	49.178	49.177	49.144	49.148	49.148	0.030	0.031	0.030
15	49.176	49.187	49.183	49.157	49.163	49.163	0.019	0.024	0.020
20	49.187	49.194	49.192	49.156	49.163	49.164	0.030	0.031	0.028

the total cost without hardening measures, illustrating that for large transmission network, implementation of hardening without differential segmentation may result in excessive investment. On the contrary, hardening 5 lines with strategy 1 achieves the lowest total cost 49.164B¥ among the 20 cases, illustrating that a proper design of the segmentation strategy and hardening budget can effectively coordinate the resilience and economic efficiency.

iv). None of the 15 case studies show both economic and resilience indicators being the highest or lowest simultaneously, indicating that there is no hardening strategy that is superior or inferior in both economic and resilience aspects.

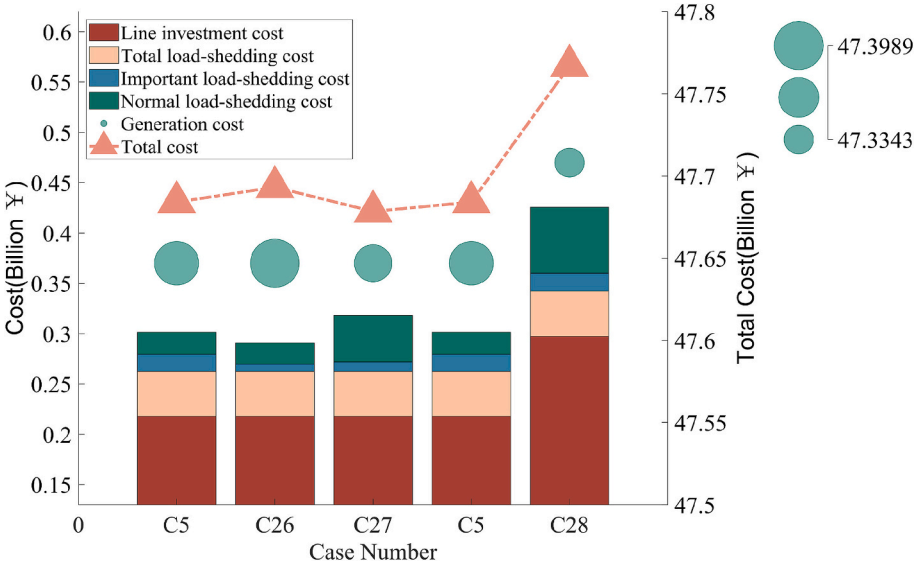

Fig. 15. Costs with different parameter settings of other short-term measures.

5.4.2. Sensitivity analysis of the other short-term measures parameters

In this part, two group of cases are designed. To reflect the impact of preventive unit commitment, we construct Case 26 (C26) without preventive unit commitment to compare with C5. This implies that the unit commitment under TDS remains consistent with that under NOS. To reflect the impact of differential load-shedding, we design Case 27 (C27) ~ Case 28 (C28), with 0 %, 100 % important load to compare with C5 (20 % important load), The costs are presented in Fig. 15.

In contrast to C5, C26, which ignores preventive unit commitment, exhibits a 0.018B¥ higher generation cost, 0.009B¥ higher total cost and 0.011B¥ lower load-shedding cost. Preventive unit commitment is shown to achieve a more cost-effective planning scheme. To further investigate the startup patterns of units under TDS, we report the 24-h unit commitment outcome under TDS of C26 and C5 in Appendix C Fig.C.1, and also present the cumulative shutdown hours for each unit over a 24-h period under the TDS for C15 and C5 in Fig. 16. It can be observed that the units situated in areas influenced by typhoon, specifically those at nodes 16, 28, have obviously reduced shutdown hours under TDS.

By comparison of C27, C5 and C28, it can be seen that the important load percentage increases from 0 % to 100 %, the total cost increases from 47.678B¥ to 47.767B¥, the line investment rises from 0.218B¥ to 0.298B¥; the cost of important load shedding increases from 0.009B¥ to 0.018B¥, while the generation cost and cost of normal load shedding show no clear trend of increase or decrease. These results indicate that the planning model without consideration of differential load-shedding may overestimate or underestimate the impact of typhoon disasters, and the differential load-shedding strategy can objectively reflect the impact of typhoon disasters, making the planning model more in line with the reality.

5.5. The Chinese 81-Bus Test system and planning results

The 81-bus 500 kV transmission system located in a Chinese province with an area of 105,500 km^2 consists of 166 existing and 130 candidate transmission lines, 29 traditional power plant. The detailed system parameters setting are presented in Appendix D. The system topology and typhoon dynamics are shown in Appendix Fig. D. 1. Eight cases are designed to verify the effectiveness of the proposed model in the 81-bus system. The first five cases are the same setting with the comparative analysis part of 30-bus system, where we verify the multi-scenario, distributionally robust and CVaR settings of the proposed model. The last three cases are designed to verify the impact of the source-network-load short-term measures settings of the proposed model, including the proposed model without preventive unit commitment, the proposed model without differential hardening (that is, hardening 15 lines with strategy 2), and the proposed model without differential load-shedding (that is, all loads are important load), the results are reported in Table 7, from which we can draw conclusions.

i). By comparison of models without multi-scenario and distributionally robust settings, the proposed model obtains the lower total cost 52.008B¥ and investment cost 0.540B¥, indicating that the proposed multi-scenario distributionally setting can effectively coordinate the resilience and economy. In contrast to model without CVaR setting, the total cost and load-shedding cost of the proposed model are 0.026B¥ and 0.016B¥ higher, illustrating that the ignorance of turbine failure risk may overestimate the OWF output under TDS and underestimate the impact of typhoon disasters.

ii). By comparison of models without preventive unit commitment, differential hardening and differential load-shedding, the total cost the proposed model proposed model decreases 0.05B¥, 0.016B¥ and 0.029B¥, respectively, and the investment cost also decreases 0.066B¥, 0.045B¥ and 0.082B¥, respectively, indicating that the source-network-load short-term measures settings successfully reduce the model conservatism.

6. Conclusion

This paper proposes a multi-scenario distributionally robust model for ROWF&TNIP considering both TDS and NOS. The proposed planning model not only takes into account the uncertainty differences in OWF output between NOS and TDS, but also captures the probability distribution uncertainties of four types of faults under both TDS and NOS. This approach comprehensively reflects the impact of NOS and TDS on planning process, and prevents overestimating TDS leading to excessive investment or underestimating TDS resulting in severe load-shedding. The coordination of transmission planning, OWF integration, and short-term measures like preventive unit commitment, differential load-shedding and differential hardening effectively enhances resilience while mitigating total investment. Specifically, the differential

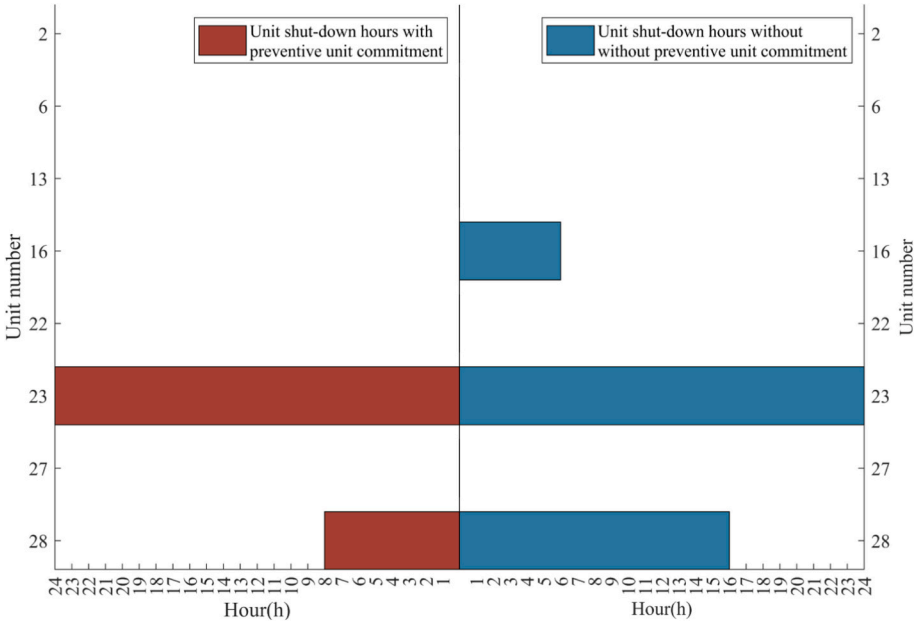

Fig. 16. Cumulative shutdown hours for each unit under TDS with and without preventive unit commitment.

Table 7
Results of ROWF&TNIP based on Different Model in 81-bus System.

81-bus system ROWF&TNIP results (B¥)	Total Cost	Investment Cost	Hardening Cost	Generation Cost	Load-shedding Cost
Single scenario distributionally robust model (No TDS)	55.099	0.081	0.213	53.804	3.441
Single scenario distributionally robust model (No NOS)	52.019	0.585	0.213	53.957	0.051
Multi-scenario robust model	52.028	0.618	0.213	53.993	0.013
Multi-scenario distributionally robust model (No CVaR)	51.982	0.585	0.213	53.992	0.047
The proposed multi-scenario distributionally robust model	52.008	0.540	0.213	53.791	0.063
The proposed model without preventive unit commitment	52.058	0.606	0.213	53.789	0.050
The proposed model without differential hardening	52.024	0.585	0.249	53.811	0.015
The proposed model without differential load-shedding	52.037	0.622	0.213	53.787	0.011

hardening model tackles the challenge of synchronizing intricate hardening model with planning measure, and compared to the non-differential hardening model, it tends to achieve lower economic costs and better resilience enhancement effects. In case study section, a series of comparative analyses and sensitivity analyses are conducted in IEEE 30-bus and an actual 81-bus system to reveal that: 1) the multi-scenario distributionally robust setting can effectively coordinate the resilience enhancement and economy efficiency; 2) the preventive unit commitment, differential hardening and differential load-shedding successfully reduce the model conservatism, and 3) it is not the case that the more lines are hardened, the better the resilience can be enhanced. It is essential to design an appropriate segmentation hardening strategy to obtain a more cost-effective planning scheme. The promising future researches may include: 1) combine ROWF&TEP model with measures in different resilience phase, such as recovery measures, 2) integrate more long-term and short-term measures into planning model, such as energy system, demand response and so on.

CRediT authorship contribution statement

Yang Yuan: Writing – original draft, Software, Resources, Methodology, Data curation, Conceptualization. **Heng Zhang:** Resources, Investigation, Funding acquisition. **Shenxi Zhang:** Investigation, Funding acquisition. **Haozhong Cheng:** Validation. **Fangping Chen:** Validation. **Zheng Wang:** Visualization. **Xiaohu Zhang:** Writing – review & editing.

Declaration of Competing Interest

The authors declare that they have no known competing financial interests or personal relationships that could have appeared to influence the work reported in this paper.

Appendix A. Appendix

The detailed descriptions of typhoon stages corresponding to each time interval in Fig. 2(b) are outlined as follows

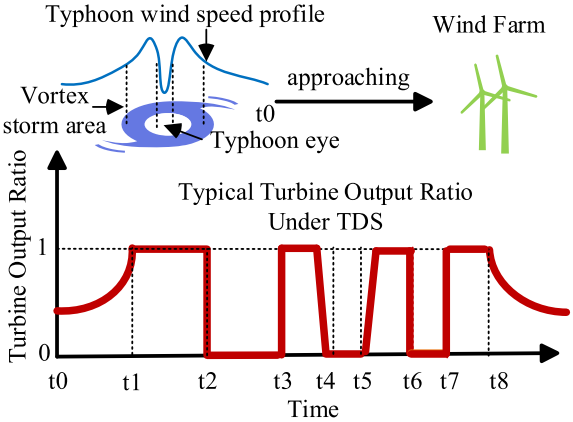

Fig. 15. (b) Typical turbine output ratio under TDS.

From t0 to t1: Starting from t0, the typhoon gradually approaches the wind turbine, and the wind speed gradually increases. At t1, the rated wind speed of the wind turbine is reached, and the wind turbine output reaches the rated output power.

From t1 to t2: The typhoon continues to approach the wind turbine, and the wind speed continues to increase. At t2, the wind turbine reaches the cut-off wind speed, and the wind turbine output is 0, but the wind turbine has not yet entered the maximum wind speed radius of the typhoon.

From t2 to t3: The turbine gradually enters the maximum wind speed radius of typhoon, and the wind speed experienced by the turbine first increases and then decreases to the cut-off wind speed at t3.

From t3 to t4: The turbine gradually approaches the eye of the typhoon, and the wind speed experienced by the turbine decreases from the cut-off wind speed at t3 to the cut-in wind speed at t4.

From t4 to t5: The typhoon eye passes through the turbine, and the wind speed decreases first, reaching its lowest point at the eye before increasing again. At time t5, the cut-in wind speed is reached.

From t5 to t6: The typhoon eye continues to move away from the turbine, but the turbine has not yet left the maximum wind speed radius range. The turbine output increases to the rated power with the increase of wind speed and is maintained until t6, when the wind speed increases to the cut-off wind speed and the output is 0.

From t6 to t7: The turbine passes through and then moves away from the maximum wind speed radius of the typhoon, and the wind speed increases and then decreases until t7, when it decreases to the cut-off wind speed. From t6 to t7, the turbine output remains zero.

From t7 to t8: The typhoon continues to move away from the turbine, and the wind speed decreases from the cut-off wind speed to the rated wind speed, while the turbine maintains its rated output power.

After t8, as the typhoon moves away from the turbine, the wind speed continues to decrease, and the turbine output decreases.

Appendix B. Appendix

Table B1
IEEE 30 bus system unit parameters.

The generator bus	Maximum output/MW	Minimum output/MW	minimum continuous shutdown/ startup time /h	Fuel cost/(¥/kWh)	Startup cost/¥
2	2000	600	2	0.31	20,000
6	6000	1800	5	0.29	300,000
13	2000	600	2	0.31	20,000
16	2500	750	3	0.31	20,000
22	5500	1650	4	0.30	30,000
23	1500	450	2	0.32	10,000
27	3000	900	3	0.31	60,000
28	1500	450	2	0.32	10,000

Table B2
wind speed interval and the corresponding hardening level and cost for hardening strategy 1.

Wind speed interval(m/s)	Hardening level (m/s)	Hardening cost(M¥/(km·year))
[0,31]	27	0.1
(31,35]	29	0.2
(35,39]	31	0.3
(39,43]	33	0.6
(43,47]	35	0.7
(47,53]	37	0.8

Table B3
wind speed interval and the corresponding hardening level and cost for hardening strategy 3.

Wind speed interval(m/s)	Hardening level (m/s)	Hardening cost(M¥/(km·year))
[0,31]	33	0.6
(31,35]	33	0.6
(35,39]	33	0.6
(39,43]	33	0.6
(43,47]	37	0.8
(47,53]	37	0.8

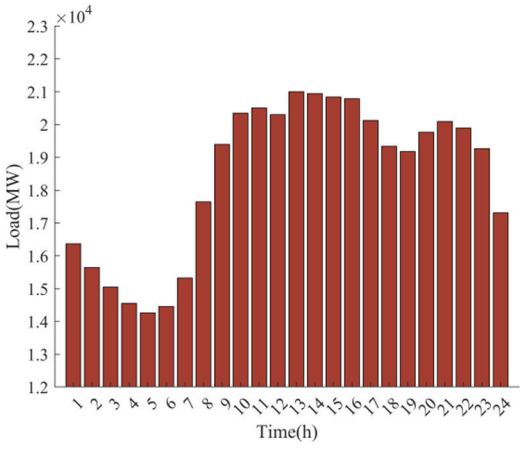

Fig. B1. Load curve of 30-bus system.

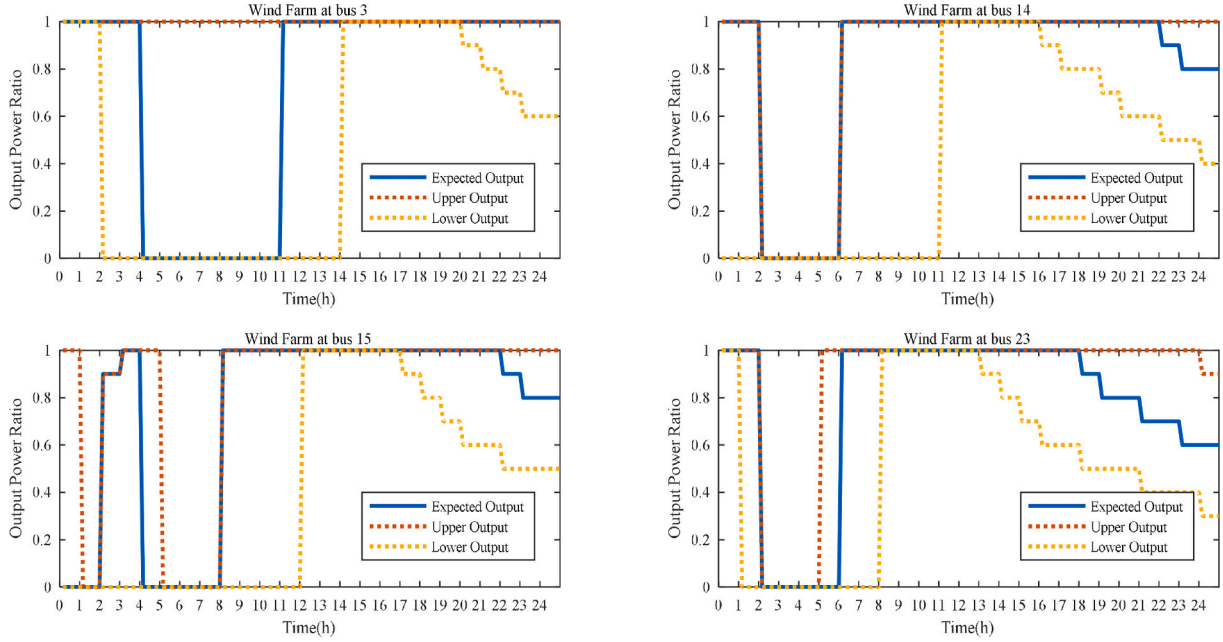

Fig. B2. Four typical turbine output curves of OWF under TDS.

Appendix C. Appendix

Equation Section (Next) The detailed form of multi-scenario robust model

(1) Objective Function

$$\min_{\substack{x_l, x_W, u^S_{gst}, \\ u^D_{gst}, u^L_{gst} \in G}} \left\{ f_1 + \max_{\substack{p_s(Z_s) \in \hat{\Omega}_{GF-Robust} \\ p_{Wst} \in \Omega_{WFO}}} \left[\sum_{s=1,2} p_s \min_{\substack{p_{gst}, p_{lst}, p_{rwst}, \\ p_{r1st}, p_{r2st} \in H}} f_2(Z_i) \right] \right\} \tag{C.1}$$

$$f_1 = \sum_{l \in L_c} C^L_l x_l + \sum_{W \in L_W} C^{OWF}_W x_W + C^H + \sum_{s=1,2} \sum_{t \in T} \sum_{g \in G} \left(C^S_g u^S_{gst} + C^D_g u^D_{gst} \right) \tag{C.2}$$

$$f_2 = \sum_{s=1,2} \sum_{t \in T} \left[\sum_{g \in G} C^G_g p_{gst} + \sum_{r_w \in L_W} C^{WC}_{r_w} p_{r_w st} + \sum_{r_1, r_2 \in B} \left(C^{LS}_{r_1} p_{r_1 st} + C^{LS}_{r_2} p_{r_2 st} \right) \right] \tag{C.3}$$

The main differences of this objective function (C.1) and that of the proposed model lie in:

a) The decision variable in the middle level here is the N—K fault Z_i which causes high loss, while in the proposed model, the decision variable is the probability distribution $p_s(Z_s)$ of four types faults. Accordingly, the fault uncertainty set $\Omega_{GF-Robust}$ in the middle level is also different from the Ω_{GF}. $\Omega_{GF-Robust}$ is the N—K fault uncertainty set, the detailed form is presented in the subsequent part. Due to this difference, in each iteration, the robust model updates N—K fault Z_i, while the proposed model updates the probability distribution of faults $p_s(Z_s)$.

b) The probability of each scenario p_s is different from the$p_s(Z_s)$. In the proposed model, $p_s(Z_s)$ is the decision variable of the middle level, whilep_s here is a given value. In the robust model which ignores the probability uncertainty, there are only two scenarios, one is the normal scenario and the other is the typhoon scenario, and p_s is determined according to the proportion of normal and typhoon days within a year. For example, if we assume 20 typhoon days within a year, that is T_D=20, then $p_{s=1} = 345/365$ and $p_{s=2} = 20/365$.

(2) Constraints.

The majority of the constraints of the robust model are the same with the proposed model, except for the fault uncertainty set in the middle level. The robust model consists of two scenarios. $s = 1$ represents the normal scenario where no fault occurs, while $s = 1$represents typhoon scenarios where a high-loss N—K fault will occur. Therefore, the fault uncertainty set is also presented in a multi-scenario form as (C.4).

$$\Omega_{GF-Robust} = \begin{cases} \sum_{l\in L} z_l = N_L, s = 1 \\ \sum_{l\in L} z_l \geqslant N_L - K_{max}, s = 2 \end{cases} \tag{C.4}$$

The detailed form of the proposed model without CVaR setting:

The only difference between the proposed model and the proposed model without CVaR setting lies in the OWF output uncertainty set. For the proposed model without CVaR setting, the OWF output uncertainty set $\Omega_{WFO}$is denoted as (C.5).

$$\Omega_{WFO} = \left\{ p_{Wst} \left| \begin{array}{l} k_2^T p_{Wst}^{TH} \leqslant p_{Wst} \leqslant k_1^T p_{Wst}^{TH}, s \in S_T \\ k_2^N p_{Wst}^{TH} \leqslant p_{Wst} \leqslant k_1^N p_{Wst}^{TH}, s \in S_N \\ p_{Wst} = N_W p_{wst}, p_{Wst}^{TH} = N_W p_{wst}^{TH} \\ k_1^T, k_1^N \in [1, +\infty), k_2^T, k_2^N \in (0, 1] \end{array} \right. \right\} \tag{C.5}$$

Table C1
The corresponding relationship between the line number and the starting-end node.

No.	Starting-end node	No.	Starting-end node	No.	Starting-end node	No.	Starting-end node
6	2–6	11	6–9	22	15–18	27	10–21
7	4–6	15	4–12	23	18–19	30	15–23
8	5–7	18	12–15	24	19–20	32	23–24
9	6–7	19	12–16	25	10–20	40	8–28
10	6–8	21	16–17	26	10–17	41	6–28

(a) preventive unit commitment (b) No preventive unit commitment.

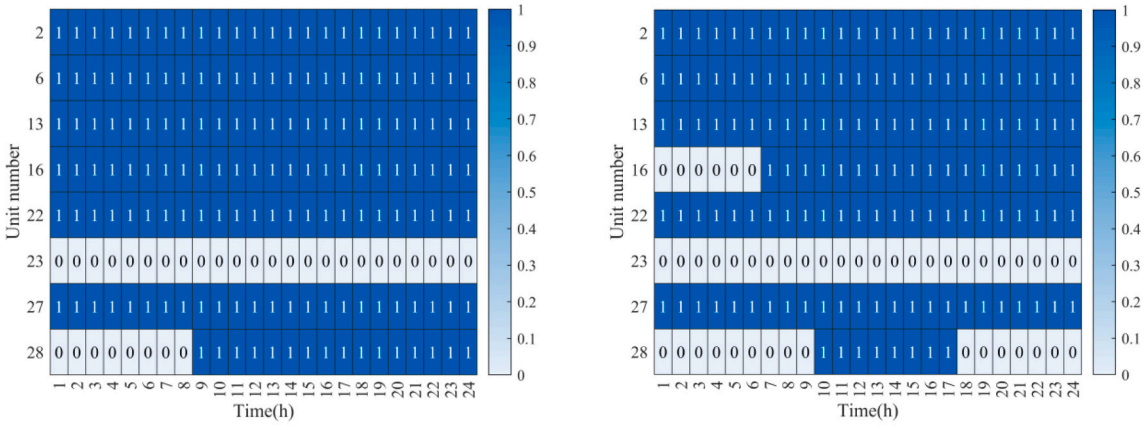

(a) preventive unit commitment (b) No preventive unit commitment

Fig. C1. Results of unit commitment with and without preventive unit commitment.

Appendix D. Appendix

The 81-bus 500 kV transmission system located in a Chinese province with an area of 105,500 km^2 consists of 166 existing and 130 candidate transmission lines, 29 traditional power plant totaling 87,637 MW generation capacity (including 24,000 MW of external UHVDC power), 1100 MW photovoltaic capacity, 7200 MW OWF to be integrated, and 83,301 MW peak load. According to the OWF integration plan of this province, 6 out of 12 potential connection buses (bus 7, 17, 18, 19, 20, 50, 51, 55, 59, 60, 61, 70) will be selected, with each bus integrating 1200 MW OWF. The simulated typhoon follows a historically typical path, making landfall at bus 51 along the southeast coast at the 4th hour with 15 km/h moving speed and 52 m/s initial max wind speed. The 81-bus system topology and the typhoon dynamics are presented in Fig. D. 1, where the load node is marked with red color. the confidential level β is 95 %. The normal and important load-shedding cost are 5¥/kWh, and 25¥/kWh**.** The other parameter settings are the

same with the IEEE 30-bus system

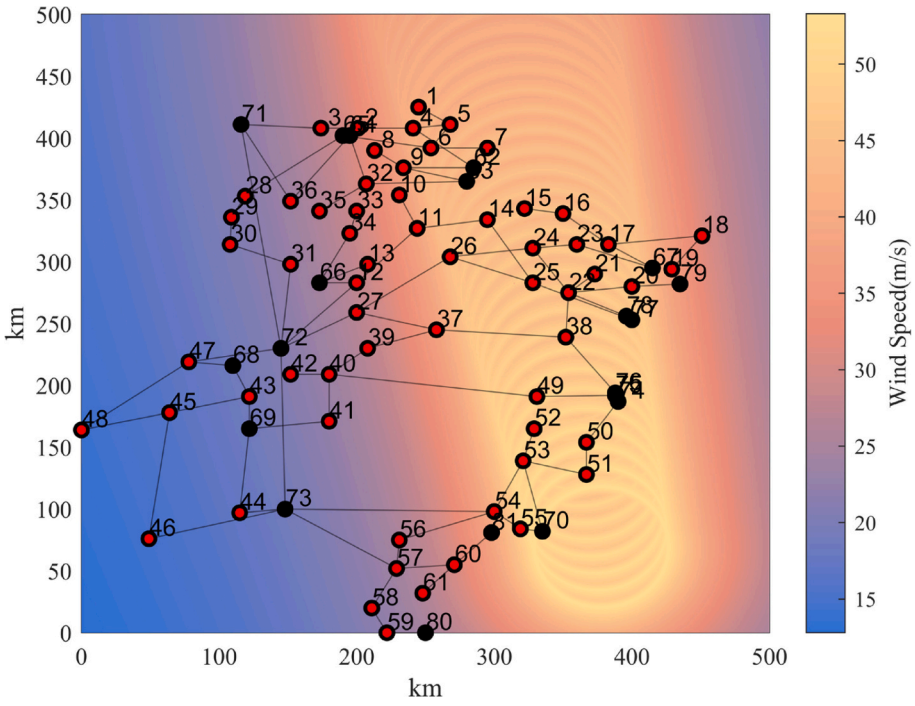

Fig. D1. 81-bus system and the typhoon trajectory.

Data availability

Data will be made available on request.

References

[1] Su R, Chen B, Wang S, Duan C. Energy technical resilience assessment based on complex network analysis – a case study of China. Appl Therm Eng 2024;364:123231.

[2] Zhang C, Wang Y, Zheng T, Zhang K. Complex network theory-based optimization for enhancing resilience of large-scale multi-energy system. Appl Therm Eng 2024;370:123593.

[3] Yuan Z, Zhang H, Cheng H, Zhang S, Zhang X, Lu J. Low-carbon oriented power system expansion planning considering the long-term uncertainties of transition tasks. Energy 2024;307:132759.

[4] Zhang H, Zhang S, Cheng H, Zheng L, Gu Q, Tian X. Boosting the power grid resilience under typhoon disasters by coordinated scheduling of wind energy and conventional generators. Renew Energy 2022;200:303–19.

[5] Zhang B, Zhang Z. A robust model for scheduling power productions of multiple offshore wind farms using one-to-many maintenance services. IET Renew Power Gener 2021;15(13):2997–3013.

[6] Zhang B, Xu G, Zhang Z. A holistic robust method for optimizing multi-timescale operations of a wind farm with energy storages. J Clean Prod 2022;356:131793.

[7] Zhang B, Wu C, Xu G, Zhang Z. A data-driven optimization model for generating robust templates of scheduling offshore wind farm maintenance tasks. Susta Energ Grids and Networks 2024;37:101250.

[8] Liang Y, Lin S, Feng X, Liu M, Su L, Zhang B. Optimal resilience enhancement dispatch of a power system with multiple offshore wind farms considering uncertain typhoon parameters. Int J Electr Power Energy Syst 2023;153:109337.

[9] Chao H, Hu B, Xie K, Tai HM, Yan J, Li Y. A sequential MCMC model for reliability evaluation of offshore wind farms considering severe weather conditions. IEEE. Access 2019;7:132552–6.

[10] Yuan Z, Zhang H, Cheng H, et al. Resilience enhancement of coordinated transmission and distribution system via risk-based decentralized planning against typhoons. IEEE Trans Ind Appl 2025. https://doi.org/10.1109/TIA.2025.3546909.

[11] Dehghani F, Mohammadi M, Karimi M. Age-dependent resilience assessment and quantification of distribution systems under extreme weather events. Int J Electr Power Energy Syst 2023;150:109089.

[12] Lian X, Qian T, Li Z, Chen X, Tang W. Resilience assessment for power system based on cascading failure graph under disturbances caused by extreme weather events. Int J Electr Power Energy Syst 2023;145:108616.

[13] Li K, Ma J, Gao J, et al. Resilience assessment of urban distribution network under heavy rain: a knowledge- informed data-driven approach. IEEE Access 2023;11:63741–50.

[14] Zhou Y, Li X, Han H, Wei Z, et al. Resilience-oriented planning of integrated electricity and heat systems: a stochastic distributionally robust optimization approach. Appl Therm Eng 2024;353:122053.

[15] Wang C, Ju P, Lei S, et al. Markov decision process-based resilience enhancement for distribution systems: an approximate dynamic programming approach. IEEE Trans Smart Grid May 2020;11(3):2498–510.

[16] Yu S, Wei C, Fang F, et al. Resilience assessment of electric-thermal energy networks considering cascading failure under ice disasters. Appl Therm Eng 2024;369:123533.

[17] Li Y, Lei S, Sun W, et al. A Distributionally robust resilience enhancement strategy for distribution networks considering decision-dependent contingencies. IEEE Trans Smart Grid 2024;15(2):1450–65.

[18] Yan J, Hu B, Xie K, et al. Data-driven transmission defense planning against extreme weather events. IEEE Trans Smart Grid 2020;11(3):2257–70.

[19] Hossain E, Roy S, Mohammad N, et al. Metrics and enhancement strategies for grid resilience and reliability during natural disasters. Appl Therm Eng 2021;290:116709.

[20] Firoozjaee MG, Sheikh-El-Eslami MK. A hybrid resilient static power system expansion planning framework. Int J Electr Power Energy Syst 2021;133(7):107234.

[21] Hamidreza Hamidpour H, Sasan P, Sheila S, Mohammadali N, Matti L. Multi-objective resilient-constrained generation and transmission expansion planning against natural disasters. Int J Electr Power Energy Syst 2021;132:107193.

[22] Shivaie M, Moghadam MK, Weinsier PD. Resilience-based tri-level framework for simultaneous transmission and substation expansion planning considering extreme weather-related events. IET Gener Transm Distrib 2020;14(16):3310–21.

[23] Saravi VS, Kalantar M, Anvari-Moghaddam A. Resilience-constrained expansion planning of integrated power–gas–heat distribution networks. Appl Therm Eng 2022;323:119315.

[24] Li T, Han X, Wu W, Sun H. Robust expansion planning and hardening strategy of meshed multi-energy distribution networks for resilience enhancement. Appl Therm Eng 2023;341:121066.

[25] Puspendu G, Mala D. Resilience-oriented planning for active distribution systems: a probabilistic approach considering regional weather profiles. Int J Electr Power Energy Syst 2024;158:109976.

[26] Faramarzi D, Rastegar H, Riahy GH, Doagou-Mojarrad H. A three-stage hybrid stochastic/IGDT framework for resilience-oriented distribution network planning. Int J Electr Power Energy Syst 2023;146:108738.

[27] Hou H, Tang J, Zhang Z, Wang Z, Wei R, Wang L, et al. Resilience enhancement of distribution network under typhoon disaster based on two-stage stochastic programming. Appl Therm Eng 2023;338:120892.

[28] Hu Q, Li G, Sun S, Bie Z. Incorporating catastrophe insurance in power distribution systems investment and planning for resilience enhancement. Int J Electr Power Energy Syst 2024;155:109438.

[29] Batts ME, Cordes MR, Russell LR, et al. Hurricane wind speeds in the United States. J Struct Div 1980;106(10):2001–16.
[30] Billinton R, Chowdhury A. Incorporation of wind energy conversion systems in conventional generating capacity adequacy assessment. IEEE Proceedings C - Gener, Trans Distri 2002;139(1):47–56.
[31] Ran X, Zhang J, Liu K. An interval–probabilistic CVaR (IP-CVaR) and modelling for unknown probability distribution of some random variables. IEEE Trans Power Syst May 2023;38(3):2035–45.
[32] Luo Z, Liu H, Wang N, et al. Optimal adaptive decentralized under-frequency load shedding for islanded smart distribution network considering wind power uncertainty. Appl Therm Eng 2024;365:123162.
[33] Yang Y, Tang W, Yang Liu, et al. Quantitative resilience assessment for power transmission systems under typhoon weather. IEEE Access 2018;6:40747–56.
[34] Min O, Dueñas-Osorio L, Min X. A three-stage resilience analysis framework for urban infrastructure systems. Struct Saf 2012;36:23–31.